ARTICLE

https://doi.org/10.1038/s41586-019-1647-8

Regulation of lifespan by neural excitation and REST

Joseph M. Zullo[1,6], Derek Drake[1,6], Liviu Aron[1], Patrick O'Hern[1], Sameer C. Dhamne[2], Noah Davidsohn[1], Chai-An Mao[3], William H. Klein[4], Alexander Rotenberg[2], David A. Bennett[5], George M. Church[1], Monica P. Colaiácovo[1] & Bruce A. Yankner[1]*

The mechanisms that extend lifespan in humans are poorly understood. Here we show that extended longevity in humans is associated with a distinct transcriptome signature in the cerebral cortex that is characterized by downregulation of genes related to neural excitation and synaptic function. In *Caenorhabditis elegans*, neural excitation increases with age and inhibition of excitation globally, or in glutamatergic or cholinergic neurons, increases longevity. Furthermore, longevity is dynamically regulated by the excitatory–inhibitory balance of neural circuits. The transcription factor REST is upregulated in humans with extended longevity and represses excitation-related genes. Notably, REST-deficient mice exhibit increased cortical activity and neuronal excitability during ageing. Similarly, loss-of-function mutations in the *C. elegans* REST orthologue genes *spr-3* and *spr-4* elevate neural excitation and reduce the lifespan of long-lived *daf-2* mutants. In wild-type worms, overexpression of *spr-4* suppresses excitation and extends lifespan. REST, SPR-3, SPR-4 and reduced excitation activate the longevity-associated transcription factors FOXO1 and DAF-16 in mammals and worms, respectively. These findings reveal a conserved mechanism of ageing that is mediated by neural circuit activity and regulated by REST.

Studies in invertebrate and mammalian models suggest that the nervous system plays a role in the regulation of ageing[1,2]. In the nematode *C. elegans*, ablation of specific sensory or neurosecretory neurons alters lifespan[3–6], and lifespan extension from reduced insulin/IGF-like signalling can be reversed by restoring function specifically in neurons[7]. However, whether the activity state of the nervous system affects the ageing process is unclear. Here we describe a conserved mechanism of ageing that is mediated by global neural activity and regulated by REST.

Neural excitation and longevity

Previous studies of the ageing human brain have shown dynamic changes in gene expression that distinguish young adults from the ageing population[8]. However, the recent expansion of data from ageing human cohorts has enabled partitioning of the ageing population into subgroups based on transcriptome profiling. To gain insight into changes in gene expression in the brain that are associated with extended human longevity, we analysed RNA sequencing (RNA-seq)[9,10] and microarray data[11] from the frontal cortex of aged individuals with intact cognitive function in three cohorts: ROSMAP, CommonMind Consortium (CMC), and Gibbs. We compared age-associated genes between all individuals and derived Pearson correlation coefficients. Hierarchical clustering suggested that the ageing population partitioned into three groups (Extended Data Fig. 1a–c). The most significant changes associated with the extended longevity groups ($\geq$85 versus $\leq$80 years of age) were downregulation of genes related to neural excitation and synaptic function, and upregulation of genes involved in immune function (Fig. 1a–d, Extended Data Fig. 1d–f, Supplementary Tables 1–6). This did not change after adjusting for amyloid deposits and neurofibrillary tangles in the ROSMAP cohort (data not shown). Meta-analysis of gene ontology (GO) enrichment in each cohort indicated that terms related to excitatory, but not inhibitory, synaptic transmission were enriched in the downregulated genes (Extended Data Fig. 1g, Supplementary Table 7). These results suggest that extended human longevity may be associated with reduced excitatory neurotransmission.

To explore the neural regulation of longevity, we used *C. elegans*, a well-established model system of ageing. We monitored neural excitation in *C. elegans* by GCaMP calcium imaging in the glutamatergic ASH neurons[12]. In wild-type worms, we observed rapid, transient pulses of GCaMP fluorescence indicative of neuronal excitation (Supplementary Video 1). Calcium influx in ASH neurons increased during normal ageing from adult day 1–2 to day 12–16 (Fig. 1e). To determine the effect of decreasing calcium influx on lifespan, worms were treated with nemadipine, an inhibitor of L-type calcium channels that reduces neural excitation (Fig. 1f). Continuous treatment with nemadipine beginning at adult day 1 extended lifespan (Fig. 1g). Moreover, incubation of worms with ivermectin, an agonist of invertebrate glutamate-gated chloride channels, suppressed neural excitation and resulted in a dose-dependent extension of mean lifespan (Fig. 1h, i). Nemadipine and ivermectin also extended lifespan when administered at day 8, when feeding activity has largely abated (Extended Data Fig. 2a), suggesting that the drugs do not act through caloric restriction. Furthermore, worm motility was preserved (Extended Data Fig. 2b, Supplementary Videos 4–6). These results suggest that global inhibition of neural excitation extends lifespan in *C. elegans*.

To explore the neural systems that mediate lifespan, we expressed a transgenic *Drosophila* histamine-gated chloride channel (HisCl1) in different neuronal populations in *C. elegans*[13]. Addition of histamine, which is not endogenously produced by worms, activates HisCl1 and inhibits neural excitation. First, we expressed HisCl1 under the control of a pan-neuronal promoter. Continuous incubation with histamine beginning on adult day 1 or day 8 extended mean lifespan (Extended Data Fig. 3a, b, i). Histamine had no effect on the lifespan of wild-type worms that did not express HisCl1 (Supplementary Table 22).

[1]Department of Genetics, Harvard Medical School, Boston, MA, USA. [2]F. M. Kirby Neurobiology Center, Department of Neurology, Boston Children's Hospital, Harvard Medical School, Boston, MA, USA. [3]Department of Ophthalmology and Visual Science, The University of Texas McGovern Medical School, Houston, TX, USA. [4]Department of Systems Biology, The University of Texas MD Anderson Cancer Center, Houston, TX, USA. [5]Rush Alzheimer's Disease Center, Rush University Medical Center, Chicago, IL, USA. [6]These authors contributed equally: Joseph Zullo, Derek Drake. *e-mail: bruce_yankner@hms.harvard.edu

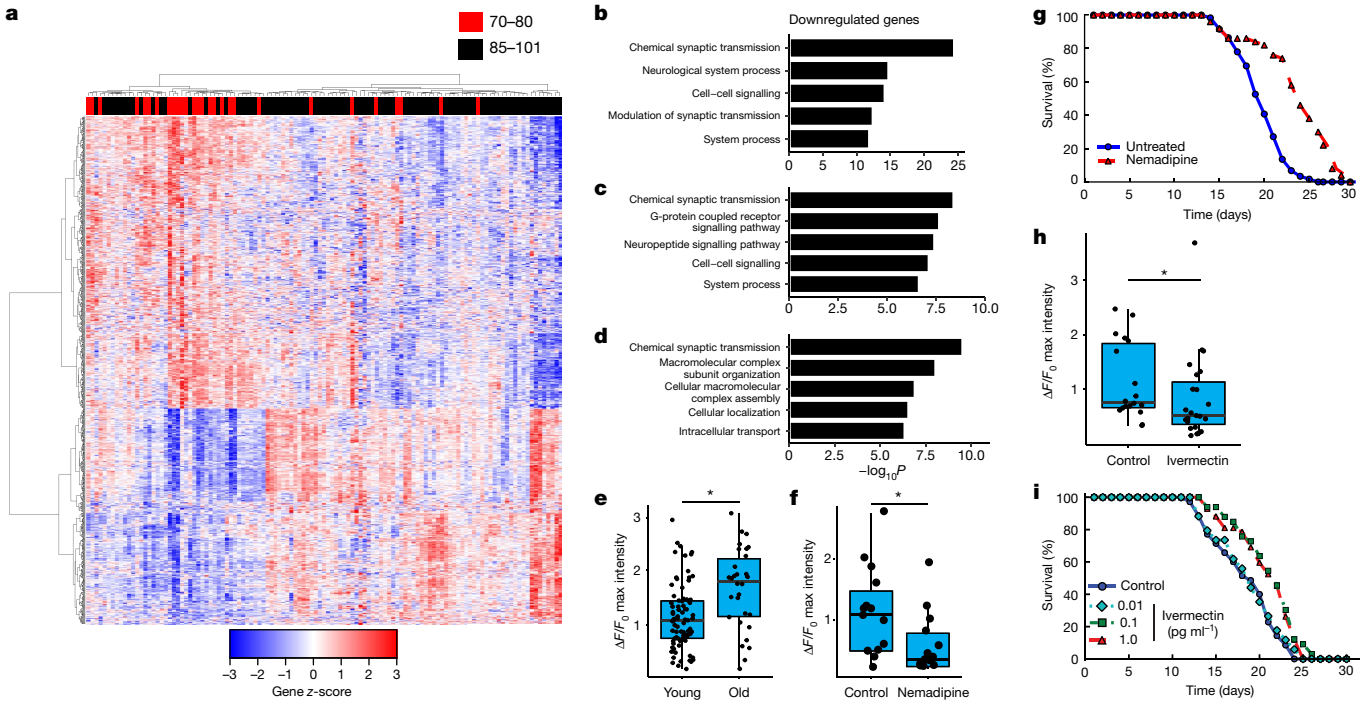

Fig. 1 | Neural excitation and longevity in humans and *C. elegans*. **a**, Analysis of the cortical transcriptome profile in cognitively intact aged individuals from the ROSMAP cohort. Unsupervised hierarchical clustering shows a transcriptional signature of downregulated and upregulated genes associated with extended longevity. **b**–**d**, Most significantly enriched gene ontology (GO) terms for downregulated genes associated with extended longevity (≥85 versus ≤ 80 years of age) in the ROSMAP (**b**; dorsolateral prefrontal cortex, $n = 117$), CMC (**c**; dorsolateral prefrontal cortex, $n = 155$), and Gibbs (**d**; frontal cortex, $n = 37$) cohorts. *P* values calculated by Fisher's exact test (see Methods). **e**, Ageing *C. elegans* exhibit increased neuronal excitation. Maximum GCaMP fluorescence intensity changes in ASH neurons of young adult (days 1–2) and older (days 12–16) worms. Young, $n = 82$ worms; old, $n = 30$ worms. $^*P = 3.6 \times 10^{-4}$ by Mann–Whitney *U*-test. In box plots: centre line, median; lower and upper hinges, first and third quartiles; upper whisker, hinge to the largest value no further than 1.5 × the interquartile range (IQR) from the hinge; lower whisker, hinge to the smallest value at most 1.5 × IQR of the hinge. **f**, The L-type calcium channel blocker nemadipine (2 μM) represses neural excitation. Control, $n = 14$; nemadipine, $n = 13$. $^*P = 0.029$, Mann–Whitney *U*-test. **g**, Nemadipine extends lifespan. Worms were continuously treated with 2 μM nemadipine beginning at adult day 1. $P = 7.7 \times 10^{-11}$, log-rank test. Control, $n = 59$; nemadipine, $n = 50$, replicated three times. **h**, The chloride channel agonist ivermectin (1 pg ml^{-1}) reduces neural excitation. Control, $n = 18$; ivermectin, $n = 23$. $^*P = 0.038$, Mann–Whitney *U*-test. **i**, Extension of lifespan by continuous treatment with ivermectin beginning at adult day 1 (control, $n = 35$; 0.01 pg ml^{-1}, $n = 34$, $P = 0.62$; 0.1 pg ml^{-1}, $n = 33$, $P = 1.5 \times 10^{-3}$; 1 pg ml^{-1}, $n = 42$, $P = 1.9 \times 10^{-3}$, log-rank test), replicated three times. Summary statistics for all individual lifespan experiments are in Supplementary Table 22.

We next expressed the HisCl1 channel in glutamatergic and cholinergic neurons, the major excitatory neuronal populations in *C. elegans*. Repression of excitation in either population robustly extended lifespan whether initiated at adult day 1 or day 8 (Extended Data Fig. 3c–f, i). Expression of HisCl1 in γ-aminobutyric acid (GABA)ergic neurons using an *unc-47* driver extended lifespan when initiated at day 1, but reduced lifespan when initiated at day 8 (Extended Data Fig. 3g–i). GCaMP imaging showed that addition of histamine to *unc-47*:HisCl1 worms at day 1 resulted in marked and persistent suppression of excitation in ASH neurons, which was not observed after addition at day 8 (Extended Data Fig. 3j). Thus, blockade of GABAergic neurotransmission early in adult life may result in compensatory downregulation of excitation in other neuronal populations. Together, these results suggest that continuous or late-life repression of neural excitation in multiple neuronal cell populations extends lifespan in *C. elegans*.

To explore the effect of hyperexcitation on lifespan, we suppressed GABAergic neurotransmission by using RNA-mediated inhibition (RNAi), which would be predicted to be less extensive than histamine/HisCl1-mediated blockade. When worms were treated with RNAi against the GABA vesicular transporter *unc-47*, there was a robust increase in excitation in ASH neurons and a reduction in lifespan (Extended Data Fig. 4a, b). Thus, the effects of neurotransmission on lifespan are bidirectional; lifespan is extended by reducing excitation and shortened by increasing excitation.

Neural activity can regulate neuropeptide secretion. To investigate the role of neuropeptide signalling in lifespan regulation, we evaluated worms in which the function of the EGL-3 proprotein convertase was blocked by an *egl-3* mutation or *egl-3* RNAi. The *egl-3* mutant exhibited robust lifespan extension (Extended Data Fig. 4c). Lifespan was also extended in worms treated with *egl-3* RNAi (Extended Data Fig. 4d), consistent with previous results[14]. Similar extension of lifespan was observed in the glutamatergic loss-of-function *eat-4* mutant and the synaptic transmission *unc-13* mutant (Extended Data Fig. 4c). These results suggest that both synaptic neurotransmission and peptidergic signalling contribute to the regulation of lifespan.

REST modulates excitation in the ageing brain

We have previously demonstrated that the transcriptional repressor REST is induced in the ageing brain[15]. Genes that were downregulated in the brain in individuals with extended longevity were enriched for the canonical REST RE1 motif in all three ageing cohorts (ROSMAP, $P = 5 \times 10^{-12}$; CMC, $P = 8 \times 10^{-4}$; Gibbs, $P = 1 \times 10^{-2}$; Supplementary Tables 1, 3, 5). Moreover, unbiased analysis by chromatin immunoprecipitation and sequencing (ChIP–seq) showed that REST was the most strongly implicated transcription factor in multiple ENCODE datasets (Supplementary Tables 8–11). Furthermore, the downregulated gene set was highly enriched for neuronal REST target genes (Supplementary Table 12). Expression of these downregulated genes, as well as an index of synaptic gene expression, were inversely related to expression of *REST* mRNA (Fig. 2a, b, Extended Data Fig. 5a, b). Furthermore, levels of REST in nuclei were elevated in prefrontal cortical neurons in centenarians relative to individuals who

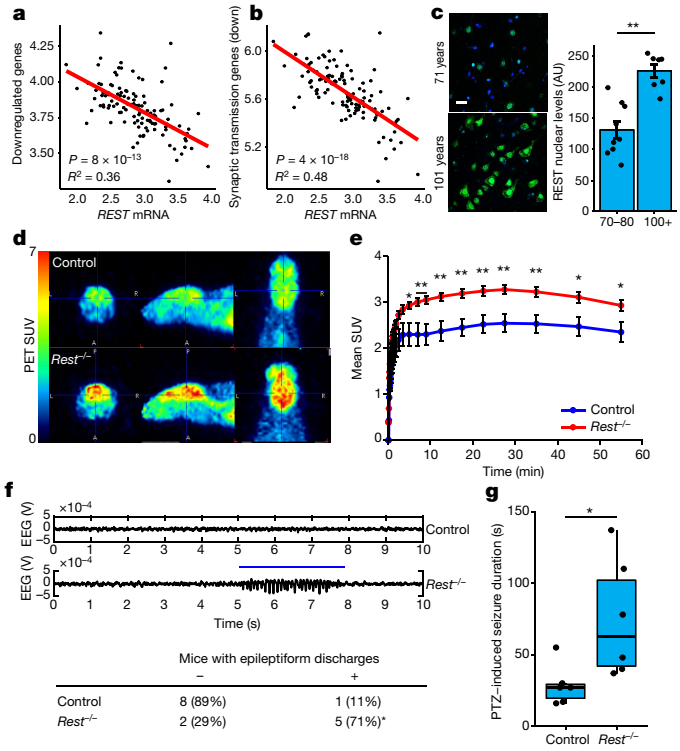

Fig. 2 | REST regulates neural excitation in the ageing brain and is associated with extended longevity. a, **b**, Expression of genes downregulated in individuals with extended longevity (≥85 versus ≤80 years old) is inversely related to levels of *REST* mRNA. Linear regression analysis of the mean expression of all downregulated genes (**a**) and downregulated genes associated with the synaptic transmission GO term (**b**). Data are from the ROSMAP cohort. Each point represents an individual case ($n = 117$). *P* values derived by *t*-tests of the regression line slopes. **c**, Increased nuclear REST levels in the prefrontal cortex of centenarians. Left, immunofluorescence labelling for REST (green, rabbit polyclonal; Bethyl laboratories) and DAPI (blue) in human prefrontal cortex. Scale bar, 40 μm. Right, nuclear REST levels in cognitively intact individuals 70–80 years ($n = 9$) and >100 years ($n = 7$) of age. AU, arbitrary units. Mean ± s.e.m., $^{**}P = 1.5 \times 10^{-4}$, Student's *t*-test. **d**, REST represses neural excitation in the mouse cerebral cortex. Shown are images from PET–CT scanning of fluorodeoxyglucose (^{18}F-FDG) uptake in 18-month-old *Nestin-Cre;Rest*$^{lx/lx}$ (*Rest*$^{-/-}$) and age-matched *Rest*$^{lx/lx}$ (control) mice. **e**, Mean ± s.e.m. standardized uptake value (SUV) at increasing time intervals after injection of ^{18}F-FDG. $n = 7$ mice per group; $^{*}P < 0.05$, $^{**}P < 0.01$; Mann–Whitney *U*-test. **f**, Increased epileptiform discharges in aged REST-deficient mice. Top, EEG recording from *Rest*$^{-/-}$ and age-matched control mice. Bottom, number of mice with at least one epileptiform discharge (≥3 s) in a 48-h recording. Control, $n = 9$; *Rest*$^{-/-}$, $n = 7$. $^{*}P = 0.035$, Fisher's exact test. **g**, Seizure duration after administration of PTZ (40 mg kg^{-1}). Control, $n = 6$; *Rest*$^{-/-}$, $n = 6$ mice. $^{*}P = 0.016$, Mann–Whitney *U*-test.

were 70–80 years of age (Fig. 2c). Although expression of *REST* mRNA is upregulated in the brain during ageing[15], increased *REST* mRNA expression did not distinguish between the extended longevity and normal ageing groups based on RNA-seq (Supplementary Tables 1, 3). However, for a given level of expression of *REST* mRNA, there is greater gene downregulation in the extended longevity group (Extended Data Fig. 5c, d). These results suggest that REST repressor function is upregulated in the brain in individuals with extended longevity, resulting in downregulation of genes that mediate excitation and synaptic function.

To assess the role of REST as a modulator of neural activity in the ageing mammalian brain, we examined the uptake of fluorodeoxyglucose (FDG) by positron emission tomography and computerized tomography (PET–CT) in the brains of 18-month-old *Nestin-Cre:Rest*$^{lx/lx}$ (*REST* conditional knockout (cKO)) mice and littermate controls[15] (Extended Data Fig. 5e). *REST* cKO mice showed elevated cortical ^{18}F-FDG uptake, indicative of increased neural activity (Fig. 2d, e). Previous studies suggest that REST can modulate excitability in mouse models of epilepsy induced by kindling or kainate[16,17]. To assess excitability during ageing, we performed electroencephalographic (EEG) recordings of *REST* cKO mice (Supplementary Table 13). Intermittent epileptiform discharges were more frequent in 22.5- to 23-month-old *REST* cKO mice than in controls (Fig. 2f). Furthermore, challenge with the GABA antagonist pentylenetetrazol (PTZ) increased seizure duration in *REST* cKO mice relative to controls (Fig. 2g), with a trend towards increased mortality (Extended Data Fig. 5f). These results suggest that REST globally represses neural activity and prevents hyperexcitation in the ageing brain.

C. elegans REST orthologues regulate longevity

The *C. elegans* gene *spr-4* encodes a structural and functional orthologue of mammalian REST that protects against toxic stressors, such as reactive oxygen species and amyloid-β protein[15]. To determine whether *spr-4* modulates lifespan, we induced endogenous expression of *spr-4* by using the RNA-guided endonuclease Cas9 as a programmable transcription factor[18]. A nuclease-deficient variant of Cas9 (dCas9) was fused to the transcriptional activator VP16 (dCas9::VP64) and stably introduced into *C. elegans* together with four small guide RNAs (sgRNAs) targeting the *spr-4* promoter. This resulted in a modest elevation in *spr-4* mRNA and protein expression, and a significant increase in mean lifespan (Extended Data Fig. 6a–d). Expression of dCas9::VP64 and *spr-4* sgRNAs in worms with the loss-of-function allele *spr-4* (*tm465*) did not affect lifespan, suggesting specificity for *spr-4* (Extended Data Fig. 6e). Moreover, overexpression of *spr-4* robustly reduced excitation in ASH neurons (Extended Data Fig. 6f). Thus, SPR-4 both represses neural excitation and extends lifespan.

The forkhead transcription factor DAF-16 is the central downstream target of the DAF-2–insulin/IGF-like signalling pathway that regulates lifespan in *C. elegans*. RNAi-mediated knockdown of *daf-16* prevented extension of lifespan by overexpression of *spr-4* (Extended Data Fig. 7a). Furthermore, extension of lifespan by the neural excitation inhibitors nemadipine and ivermectin was also dependent on *daf-16*, and ivermectin elevates both total and nuclear levels of DAF-16 (Extended Data Fig. 7b–f). Thus, DAF-16 mediates extension of lifespan by *spr-4* and neural suppression.

To further explore the effects of REST orthologues on the DAF-2–DAF-16 signalling pathway, we performed *daf-2* RNAi in wild-type worms, *spr-3* and *spr-4* loss-of-function mutants, and an *spr-4;spr-3* double mutant. As previously shown[19], *daf-2* RNAi extends lifespan by about 50% in wild-type worms. Mutations in *spr-3*, *spr-4*, or both reduced the extension of lifespan by *daf-2* RNAi (Extended Data Fig. 8a). Mutations in *spr-3* and *spr-4* also reduced the lifespan extension associated with the loss-of-function *daf-2*(*e1370*) allele; the greatest reduction occurred in the *spr-4;spr-3;daf-2* triple mutant (Fig. 3a). The *spr-3* and *spr-4* mutations did not affect lifespan in a wild-type background (Extended Data Fig. 8b), in contrast to a previous report that suggested that *spr-3* mutations altered lifespan[20]. These results suggest that *spr-3* and *spr-4* contribute to the regulation of lifespan by the insulin/IGF-like signalling pathway in worms.

We next investigated whether SPR-3 and SPR-4 function in neurons to regulate lifespan. To address this question, we used a *C. elegans* line in which RNAi was abolished by deletion of the double-stranded RNA transporter SID-1, but restored specifically in neurons by a *sid-1* transgene driven by a neuron-specific promoter[21]. These alleles were crossed into the *daf-2(e1370)* mutant background, and RNAi-mediated knockdown of both *spr-3* and *spr-4* was performed. Neuron-targeted knockdown of *spr-3* and *spr-4* significantly reduced lifespan (Fig. 3b, Extended Data Fig. 8c). Thus, neuronal expression of *spr-3* and *spr-4* contributes to lifespan extension in the *daf-2* mutant.

SPR-3 and SPR-4 regulate neural excitation

To gain further insight into the effects of SPR-3 and SPR-4 on DAF-2 function and lifespan, we performed RNA-seq on wild-type worms and

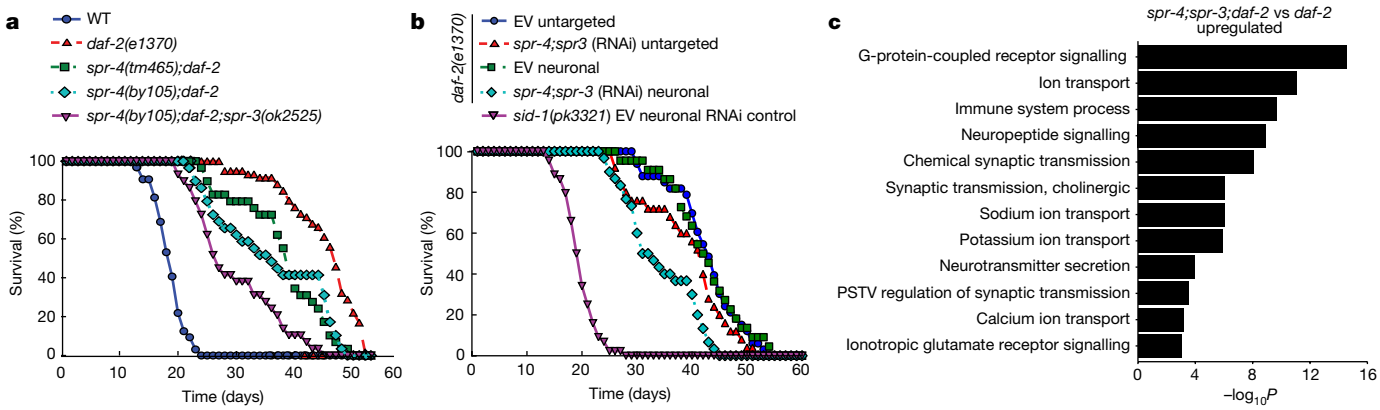

Fig. 3 | *C. elegans* REST orthologues mediate longevity in *daf*-2 loss-of-function mutants. a, The REST orthologues *spr-4* and *spr-3* are required for maximal longevity in *daf-2* mutant worms. Lifespan analysis was performed on wild-type (WT) and *daf-2(1370)* loss-of-function mutant worms, and the indicated combinations of *daf-2* and *spr-4;spr-3* mutations. The *spr-4;spr-3* mutations significantly reduced the lifespan of *daf-2* mutant worms. $n = 29$–59 worms per genotype, replicated at least three times per genotype. $P < 0.001$ for all curves relative to *daf-2*, by log-rank test. **b**, Neuronal expression of *spr-3* and *spr-4* mediate lifespan extension in *daf-2* mutant worms. Lifespans of worms with neuronal targeting of RNAi by neuronal expression of a *sid*-1 transgene in otherwise *sid-1* null *daf-2(1370)* mutants, or untargeted RNAi in *sid-1* wild-type *daf-2(1370)* mutants. Lifespan effect of neuronal targeting of *spr-4;spr-3* RNAi versus empty vector (EV) control RNAi is significant by log-rank test ($P = 2.5 \times 10^{-6}$), $n = 22$–56 worms per curve replicated at least four times. **c**, SPR-3 and SPR-4 repress genes that mediate neural excitation. Shown are significantly enriched GO terms for upregulated genes related to neural excitation in RNA-seq analysis of day 2 *spr-4;spr-3;daf-2* triple mutants versus *daf-2* single mutant worms. *P* values calculated using Fisher's exact test (see Methods), $n = 3$ biological replicates per genotype.

worms with mutations in *spr-4* and *spr-3*, *daf-2*, or *spr-4*, *spr-3* and *daf-2* (triple mutants) (Extended Data Fig. 8d, Supplementary Table 14). The comparison of triple mutant *spr-4;spr-3;daf-2* worms with single mutant *daf-2* worms was notable for highly significant changes in the transcriptome that were enriched for GO terms related to neural excitation, signalling and synaptic function (Fig. 3c, Supplementary Table 15). Furthermore, gene expression changes in *daf-2* mutants and *spr-4;spr-3* mutants overlapped (Extended Data Fig. 8e), and genes that were downregulated in *daf-2* mutants but upregulated in the *spr-4;spr-3;daf-2* triple mutants were enriched for GO terms related to neural excitation (Supplementary Table 16). These results suggest that repression of neuronal genes is a conserved regulatory feature of REST and its worm orthologues.

A central question is whether SPR-3 and SPR-4 affect lifespan by suppressing neural excitation. GCaMP calcium imaging showed that neural excitation was strongly suppressed in *daf*-2 mutants, both in young adult worms and during ageing (Fig. 4a, b, Extended Data Fig. 8f, Supplementary Videos 1–3). The *spr-4;spr-3* mutations partially restored neural excitation in *daf-2* mutants (Fig. 4a, b), but did not increase excitation in wild-type worms (Extended Data Fig. 8g). Suppression of excitation in *daf-2* mutants was not mediated by neuronal DAF-16 (Extended Data Fig. 8h). However, inhibition of neural excitation with ivermectin reversed the lifespan-shortening effect of *spr-4;spr-3* mutations in *daf-2* mutant worms (Fig. 4c). Thus, SPR-3 and SPR-4 contribute to the extreme longevity of *daf-2* mutant worms by repressing neural excitation.

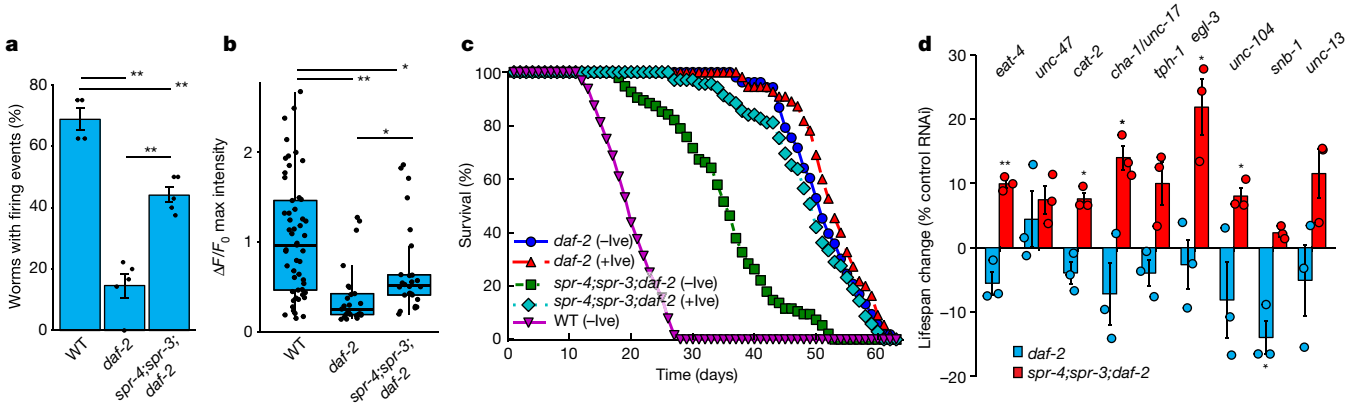

Fig. 4 | SPR-3 and SPR-4 suppress multiple neurotransmitter and neuropeptide systems to extend lifespan in *daf-2* mutant worms. **a**, Neural excitation is suppressed in *daf-2* mutants and partially restored by *spr-4;spr-3* mutations. GCaMP imaging was performed in ASH neurons. Shown is the fraction of worms with at least one firing event in a 2-min recording. Mean ± s.e.m., $n = 4$–5 independent experiments. $^{**}P = 7.9 \times 10^{-7}$ (*daf-2* versus wild-type), $P = 1.5 \times 10^{-4}$ (*spr-4;spr-3;daf-2* versus *daf-2*); $P = 0.0011$ (*spr-4;spr-3;daf-2* versus wild-type); ANOVA with post hoc Tukey test. **b**, Quantification of GCaMP fluorescence changes in day 2 worms: wild-type, $n = 53$; *daf-2*, $n = 25$; *spr-4;spr-3;daf-2*, $n = 26$. $^{**}P = 3.1 \times 10^{-6}$ (*daf-2* versus wild-type), $P = 1.5 \times 10^{-3}$ (*spr-4;spr-3;daf-2* versus *daf-2*), $^{*}P = 0.018$ (*spr-4;spr-3;daf-2* versus wild-type); Mann–Whitney *U*-test with multiple testing correction by Holm's method. **c**, Inhibition of neural excitation by ivermectin (+Ive, 10 pg ml^{-1}) reverses lifespan reduction by *spr-4;spr-3* mutations in *daf-2* mutant worms ($P = 1.1 \times 10^{-16}$ (*spr-4;spr-3;daf-2* +Ive versus −Ive)); *daf-2* −Ive, $n = 53$ worms; *daf-2* +Ive, $n = 55$; *spr-4;spr-3;daf-2* −Ive, $n = 95$; *spr-4;spr-3;daf-2* +Ive, $n = 69$; WT −Ive, $n = 64$. **d**, Multiple neurotransmitter and neuropeptide signalling systems contribute to the effects of *spr-4;spr-3* mutations on longevity. Change in lifespan of *spr-4;spr-3;daf-2* triple mutant and *daf-2* single mutant worms following neuronal RNAi of the indicated genes relative to empty vector control RNA. RNAi was targeted to neurons as described in Fig. 3b. $^{*}P < 0.05$, $^{**}P < 0.01$, Student's *t*-test. $n = 3$ independent experiments per group. Individual statistics are in Supplementary Table 22.

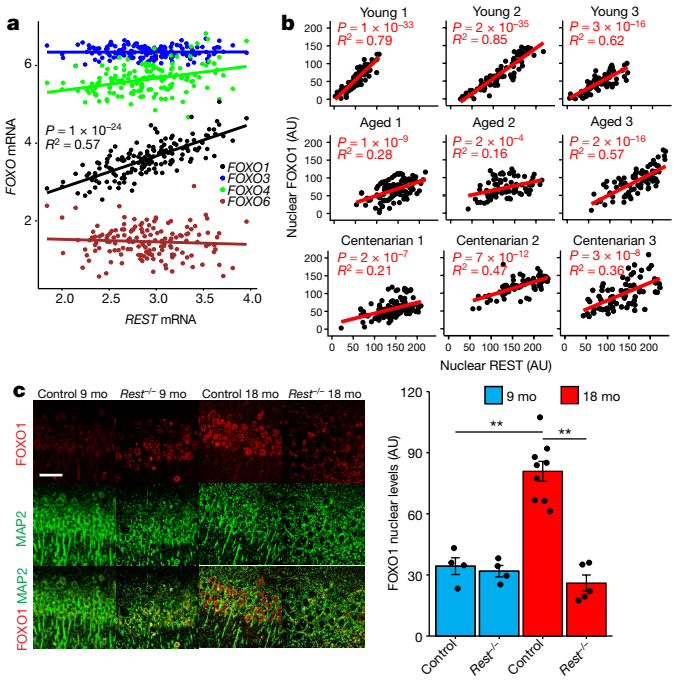

Fig. 5 | REST regulates FOXO1 expression in the mammalian brain. **a**, Linear regression analysis of *REST* and *FOXO1* mRNA expression in the prefrontal cortex of cognitively intact individuals (ROSMAP cohort age 71–101 years, $n = 150$) determined by RNA sequencing. *P* values derived by linear regression *t*-tests for the slope with Bonferroni correction for all expressed genes. **b**, Coordinate regulation of REST and FOXO1 in human prefrontal cortex. Nuclear REST and FOXO1 protein levels were determined by immunofluorescence microscopy in pyramidal neurons of the prefrontal cortex in individual young adults (20–38 years old), aged adults (70–80 years old), and centenarians (>100 years old). Each point represents a neuron that was double-labelled for REST and FOXO1. $n = 71$–114 neurons per individual. *P* values derived as in **a**. **c**, FOXO1 induction in the ageing mouse cortex is REST-dependent. Left, immunocytochemical labelling for FOXO1 and the neuronal marker MAP2 in cortical neurons of $Rest^{lx/lx}$ (control) and *Nestin-Cre*;$Rest^{lx/lx}$ ($Rest^{-/-}$) mice at 9 and 18 months (mo) of age. Scale bar, 40 μm. Right, quantification of FOXO1 nuclear levels. Mean ± s.e.m. Control 9 mo, $n = 4$ mice; control 18 mo, $n = 9$ mice; $Rest^{-/-}$ 9 mo, $n = 4$ mice; $Rest^{-/-}$ 18 mo, $n = 5$ mice. $^{**}P = 1.2 \times 10^{-5}$ control 9 mo versus control 18 mo; $^{**}P = 4.4 \times 10^{-7}$ control 18 mo versus $Rest^{-/-}$ 18 mo; ANOVA with post hoc Tukey test.

To identify the neural systems affected by SPR-4 and SPR-3, we used RNAi to target neurotransmitters and neuropeptides in *spr-4;spr-3;daf-2* triple mutants and *daf-2* single mutants. The most significant lifespan effects in the triple mutants were observed following RNAi directed against signalling through glutamatergic (*eat-4*), cholinergic (*cha-1/unc-17*) and monoaminergic (*cat-2*) neurons, and by RNAi against genes encoding axonal kinesin (*unc-104*) and the proprotein convertase (*egl-3*) (Fig. 4d, Extended Data Fig. 8i). These results suggest that SPR-3 and SPR-4 suppress excitatory neurotransmitter systems, as well as neuropeptide signalling, to extend lifespan in *daf-2* mutant worms.

Loss of function of *daf-2* extends lifespan through activation of DAF-16[22]. Following *daf*-2 RNAi, *spr-4;spr-3* mutants showed reduced total and nuclear DAF-16 levels (Extended Data Fig. 9a). RNA-seq analysis of day10 *spr-4;spr-3;daf-2* triple mutant worms showed a reduction in the expression of DAF-16 target genes relative to *daf-2* single mutants (Extended Data Fig. 9b–d, Supplementary Tables 17, 18). Furthermore, inhibition of neural excitation by ivermectin restored levels of DAF-16 in *spr-4;spr-3* mutants following *daf-2* RNAi (Extended Data Fig. 9e). Thus, SPR-3 and SPR-4 suppress neural excitation (Fig. 4a, b), which leads to the activation of DAF-16.

REST, FOXO1 and neural excitation

We next investigated whether the association between REST, neural excitation and human longevity (Fig. 2a–c) might be mediated by a mammalian forkhead transcription factor orthologous to *C. elegans* DAF-16. REST has been shown to regulate the expression of FOXO1 in SH-SY5Y neuroblastoma cells[15]. In the human brain, expression of *REST* mRNA was positively correlated with expression of *FOXO1* mRNA, but did not correlate with the expression of other FOXO family members (Fig. 5a, Extended Data Fig. 10a). Furthermore, REST and FOXO1 co-localized in neurons of the ageing human prefrontal cortex (Extended Data Fig. 10b), and nuclear levels of REST and FOXO1 were strongly positively correlated in all age groups (Fig. 5b).

To determine whether REST regulates FOXO1 expression in the brain, we examined *Rest* cKO and littermate control mice. FOXO1 localized predominantly to cortical neurons, and showed an age-related increase in 18-month-old relative to 9-month-old control mice (Fig. 5c). Age-dependent induction of nuclear FOXO1 was abolished in *Rest* cKO mice (Fig. 5c). Thus, regulation of forkhead transcription factors is a conserved feature of REST and its *C. elegans* orthologues.

To explore the role of neural excitation in regulation of FOXO1, we treated primary mouse cortical neuronal cultures with kynurenic acid (a broad-spectrum glutamate receptor antagonist) or with either 2-amino-5-phosphonovalerate (AP5) or 2,3-dihydroxy-6-nitro-7-sulfamoyl-benzo[f]quinoxaline (NBQX) (antagonists for the NMDA (*N*-methyl-D-aspartate) and AMPA (α-amino-3-hydroxy-5-methyl-4-isoxazole propionic acid)/kainate subtypes of glutamate receptor, respectively). Kynurenic acid and NBQX significantly increased nuclear and total levels of FOXO1 (Extended Data Fig. 10c). Thus, FOXO1 is regulated by glutamatergic signalling in mammalian cortical neurons, paralleling the effect of neural excitation on DAF-16 in worms.

Discussion

We have shown that extended longevity and cognitive preservation in humans is associated with coordinate downregulation of genes that mediate excitatory neurotransmission. In the model system *C. elegans*, an increase in the activity of excitatory ASH neurons is a normal aspect of ageing. Global inhibition of neural excitation, or inhibition of specific excitatory neuronal populations—particularly glutamatergic or cholinergic neurons—resulted in robust extension of lifespan. These findings are consistent with previous studies, which showed that the anticonvulsants ethosuximide and valproic acid can extend lifespan in *C. elegans*[23–25]. Moreover, we found that lifespan was dynamically regulated by the excitatory–inhibitory balance of neural circuits. Thus, an imbalance between neural excitation and inhibition might degrade neural function and contribute to the ageing process.

Our findings suggest that REST and the *C. elegans* orthologues SPR-3 and SPR-4 regulate ageing by acting as transcriptional repressors of synaptic genes and thereby reducing neural activity. Ageing conditional REST-deficient mice exhibit increased cortical neural activity and hyperexcitability. This is consistent with previous studies in neuronal cell culture, which suggested that REST maintains neural network homeostasis by buffering changes in neural excitation[26,27].

It is intriguing that REST and neural activity converge with insulin–IGF signalling to regulate the activity of forkhead transcription factors that play pivotal roles in lifespan regulation[22,28]. The activation of *daf-16* by REST orthologues in worms and *FOXO1* by REST in humans might be a mechanism for integration of neural activity with metabolism. We suggest that activation of REST and reduction of excitatory neural activity could be an approach to slowing ageing in humans.

Online content

Any methods, additional references, Nature Research reporting summaries, source data, extended data, supplementary information, acknowledgements, peer review information; details of author contributions and competing interests; and statements of data and code availability are available at https://doi.org/10.1038/s41586-019-1647-8.

Received: 28 November 2017; Accepted: 18 September 2019;
Published online 16 October 2019.

1. Satoh, A., Imai, S. I. & Guarente, L. The brain, sirtuins, and ageing. *Nat. Rev. Neurosci*. **18**, 362–374 (2017).
2. Bishop, N. A., Lu, T. & Yankner, B. A. Neural mechanisms of ageing and cognitive decline. *Nature* **464**, 529–535 (2010).
3. Ailion, M., Inoue, T., Weaver, C. I., Holdcraft, R. W. & Thomas, J. H. Neurosecretory control of aging in *Caenorhabditis elegans*. *Proc. Natl Acad. Sci. USA* **96**, 7394–7397 (1999).
4. Apfeld, J. & Kenyon, C. Regulation of lifespan by sensory perception in *Caenorhabditis elegans*. *Nature* **402**, 804–809 (1999).
5. Alcedo, J. & Kenyon, C. Regulation of *C. elegans* longevity by specific gustatory and olfactory neurons. *Neuron* **41**, 45–55 (2004).
6. Bishop, N. A. & Guarente, L. Two neurons mediate diet-restriction-induced longevity in *C. elegans*. *Nature* **447**, 545–549 (2007).
7. Wolkow, C. A., Kimura, K. D., Lee, M.-S. & Ruvkun, G. Regulation of *C. elegans* life-span by insulinlike signaling in the nervous system. *Science* **290**, 147–150 (2000).
8. Lu, T. et al. Gene regulation and DNA damage in the ageing human brain. *Nature* **429**, 883–891 (2004).
9. Mostafavi, S. et al. A molecular network of the aging human brain provides insights into the pathology and cognitive decline of Alzheimer's disease. *Nat. Neurosci*. **21**, 811–819 (2018).
10. Fromer, M. et al. Gene expression elucidates functional impact of polygenic risk for schizophrenia. *Nat. Neurosci*. **19**, 1442–1453 (2016).
11. Gibbs, J. R. et al. Abundant quantitative trait loci exist for DNA methylation and gene expression in human brain. *PLoS Genet*. **6**, e1000952 (2010).
12. Hilliard, M. A. et al. In vivo imaging of *C. elegans* ASH neurons: cellular response and adaptation to chemical repellents. *EMBO J*. **24**, 63–72 (2005).
13. Pokala, N., Liu, Q., Gordus, A. & Bargmann, C. I. Inducible and titratable silencing of *Caenorhabditis elegans* neurons in vivo with histamine-gated chloride channels. *Proc. Natl Acad. Sci. USA* **111**, 2770–2775 (2014).
14. Hamilton, B. et al. A systematic RNAi screen for longevity genes in *C. elegans*. *Genes Dev*. **19**, 1544–1555 (2005).
15. Lu, T. et al. REST and stress resistance in ageing and Alzheimer's disease. *Nature* **507**, 448–454 (2014).
16. Hu, X. L. et al. Conditional deletion of NRSF in forebrain neurons accelerates epileptogenesis in the kindling model. *Cereb. Cortex* **21**, 2158–2165 (2011).
17. Brennan, G. P. et al. Dual and opposing roles of microRNA-124 in epilepsy are mediated through inflammatory and NRSF-dependent gene networks. *Cell Rep*. **14**, 2402–2412 (2016).
18. Gilbert, L. A. et al. CRISPR-mediated modular RNA-guided regulation of transcription in eukaryotes. *Cell* **154**, 442–451 (2013).
19. Dillin, A., Crawford, D. K. & Kenyon, C. Timing requirements for insulin/IGF-1 signallling in *C. elegans*. *Science* **298**, 830–834 (2002).
20. Yang, P. et al. A C-terminal truncated mutation of *spr-3* gene extends lifespan in *Caenorhabditis elegans*. *Acta Biochim. Biophys. Sin. (Shanghai)* **45**, 540–548 (2013).
21. Calixto, A., Chelur, D., Topalidou, I., Chen, X. & Chalfie, M. Enhanced neuronal RNAi in *C. elegans* using SID-1. *Nat. Methods* **7**, 554–559 (2010).
22. Lin, K., Dorman, J. B., Rodan, A. & Kenyon, C. daf-16: An HNF-3/forkhead family member that can function to double the life-span of *Caenorhabditis elegans*. *Science* **278**, 1319–1322 (1997).
23. Evason, K., Huang, C., Yamben, I., Covey, D. F. & Kornfeld, K. Anticonvulsant medications extend worm life-span. *Science* **307**, 258–262 (2005).
24. Evason, K., Collins, J. J., Huang, C., Hughes, S. & Kornfeld, K. Valproic acid extends *Caenorhabditis elegans* lifespan. *Aging Cell* **7**, 305–317 (2008).
25. Chen, X. et al. Ethosuximide ameliorates neurodegenerative disease phenotypes by modulating DAF-16/FOXO target gene expression. *Mol. Neurodegener*. **10**, 51 (2015).
26. Pozzi, D. et al. REST/NRSF-mediated intrinsic homeostasis protects neuronal networks from hyperexcitability. *EMBO J*. **32**, 2994–3007 (2013).
27. Pecoraro-Bisogni, F. et al. REST-dependent presynaptic homeostasis induced by chronic neuronal hyperactivity. *Mol. Neurobiol*. **55**, 4959–4972 (2018).
28. Li, Y. et al. Genetic association of FOXO1A and FOXO3A with longevity trait in Han Chinese populations. *Hum. Mol. Genet*. **18**, 4897–4904 (2009).

METHODS

Brain sample procurement and description. Postmortem human brain material was procured in accordance with institutional guidelines and was approved by the Harvard Medical School Institutional Review Board. Tissue samples were procured from the Rush University Medical Center and the Brigham and Women's Hospital. Tissue samples (both paraffin-embedded and frozen) from Rush University Medical Center were derived from participants in the Religious Order Study (ROS) and Rush Memory and Ageing Project (MAP) (together referred to as ROSMAP) at the Rush Alzheimer's Disease Center; these are longitudinal, clinical–pathologic studies of ageing, cognitive decline and Alzheimer's disease[29,30]. Study participants agreed to comprehensive annual clinical and neuropsychological evaluation and to brain donation at death. Twenty-one cognitive function tests were used for the present study, including a summary score of all 17 tests used as a measure of global cognition, and separate measures of episodic, semantic, and working memory, perceptual speed, and visuospatial ability. The follow-up rate exceeds 95% and the autopsy rate exceeds 90%. All individuals who underwent autopsy cases were subject to a uniform structured neuropathologic evaluation of Alzheimer's disease, including assignment of Braak (measure of number and distribution of neurofibrillary tangles), CERAD (Aβ plaque pathology), and NIA-Reagan (composite measure of neurofibrillary tangles and amyloid plaques) scores (https://www.radc.rush.edu/docs/var/detail.htm?category=Pathology&subcategory=Alzheimer%27s%20disease&variable=ceradsc). Paraffin-embedded brain samples were also obtained from the Brigham and Women's Hospital. These samples included tissue from young adults without neurological abnormalities.

Immunofluorescence analysis of human brain. Immunofluorescence analysis of the prefrontal cortex (Brodmann areas 9, 10 and 47) was carried out using paraffin-embedded brain sections. Paraffin-embedded tissue sections were first deparaffinized in xylene, then rehydrated with decreasing concentrations of ethanol and placed in water. Sections then underwent antigen retrieval using the Diva decloaker (BioCare, USA). They were then washed and blocked with 2% BSA and 0.1% Triton X-100 in PBS for 1 h at room temperature. Primary antibodies were diluted in 2% BSA and 0.1% Triton in PBS. Following overnight incubation at 4 °C, sections were washed three times with PBS. Secondary antibodies, diluted in 2% BSA and 0.1% Triton in PBS were either biotin-coupled (1:200, Vector Labs, USA) or coupled to Alexa fluorophores (1:300, Invitrogen). Sections were incubated with 1% Sudan Black in 80% ethanol for 10 min at room temperature to suppress lipofuscin autofluorescence. Following washes in PBS, sections were mounted and imaged using confocal microscopy. The following antibodies were used for immunolabelling: (i) a rabbit polyclonal IgG that recognizes a region between residues 1050 and the C terminus (residue 1097) of REST (Bethyl laboratories, IHC-00141); (ii) a goat polyclonal IgG that recognizes the C-terminal region of FOXO1a (LSBio B415, discontinued, replaced with LSBio 1322). To quantify immunofluorescence, images that were randomly acquired in selected brain regions were analysed using the Metamorph image analysis system. Antigen-expressing areas within each neuron (such as the nucleus) were selected using the average signal intensity measured. Values were corrected by subtracting the average slide background intensity (measured outside cells). The investigator was blinded to sample origin or diagnosis.

To assess the relationship between the levels of nuclear REST protein and FOXO1, we performed confocal immunofluorescence with triple-labelling for REST, MAP2 and FOXO1. Multiple 40× pictures were acquired (at various locations) within the prefrontal cortex displaying pyramidal neurons using an Olympus Fluoview Confocal Microscope. For cases displaying a majority of pyramidal neurons with very high (or very low) nuclear REST levels, fields were also included that displayed lower (or higher, respectively) REST levels, to test for potential correlations between REST and FOXO1. Antigen-expressing areas within neuronal nuclei were selected using the Metamorph image analysis system and the average signal intensity was measured. Values were corrected by subtracting the average slide background intensity (measured outside cells). Between 70 and 115 pyramidal neurons were quantified for each case.

Conditional *Rest* knockout mice. Animal housing and experimental procedures were approved by the Institutional Animal Care and Use Committee of Harvard Medical School. Mice carrying floxed alleles of *Rest* flanking exon 2 were described previously[31,32]. These mice were crossed to *Nestin-Cre* transgenic mice (Jackson laboratory; strain 003771) to achieve conditional inactivation of *Rest* in the nervous system. The *Nes-Cre* transgene is in the C57BL/6J background, and the $Rest^{lx/lx}$ alleles were in a hybrid C57BL/6J and 129Sv/Ev background. The resulting *Nestin-Cre:*$Rest^{lx/lx}$ conditional knockout mice (hybrid C57BL/6J and 129Sv/Ev background), referred to as *Rest* cKO, were born at expected Mendelian ratios, were viable and fertile, and did not display any visible alterations. The control groups included $Rest^{lx/lx}$ and *Nes-Cre* mice. Mouse genotyping by PCR was performed using the following primers to amplify a region in the *Rest* gene flanking exon 2: re08 (5′-CATGCGAGTACTGCCATACCCAAC-3′), re09 (5′-GTGATGGGGCAGTCTTCTGGAGG-3′), and re11 (5′-GGCACACCTTTA ATCCTAGCTTC-3′); this allowed the identification of wild-type (220 bp), floxed (264 bp) or recombined (375 bp) *Rest* alleles. The experimental groups included both male and female mice in equal proportions. The *Rest* cKO and $Rest^{+/+}$ control groups were composed of littermate mice on the same genetic background. Mice were identified by eartag numbers, and were randomly selected for PET–CT and EEG experiments, as well as for histological processing (perfusion, brain dissection, and so on).

Immunofluorescence analysis of mouse brain. Mice were anaesthetized with isoflurane and carbon dioxide and then perfused with cold PBS buffer for 20 min. Brains were rapidly removed and placed in 4% PFA overnight at 4 °C. They were then processed for paraffin embedding, according to standard procedures. The investigator was blind to the genotype. To assess FOXO1 nuclear expression in cortical neurons, coronal brain sections from wild-type and *Rest* cKO mice (aged 9 or 18 months) were immunolabelled with FOXO1 and MAP2 antibodies. Cortical neurons ($MAP2^{+}$) were identified and the mean FOXO1 fluorescence intensity in each nucleus was measured using Metamorph software. Between 50 and 100 neuronal nuclei were assessed for FOXO1 expression, and the mean FOXO1 nuclear expression was derived for each animal. To confirm REST deficiency (Extended Data Fig. 5e), *Rest* cKO mouse cortical sections were labelled with an anti-REST antibody provided by the Hsieh laboratory (Supplementary Table 20).

PET–CT of *Rest* cKO mice. Mice were anaesthetized with 3% isoflurane (Baxter Medical) and medical grade oxygen at a rate of 1 l/min. A CT scout scan was done first, followed by a CT scan and a dynamic PET scan. Each mouse received the same dose per gram of body weight (1.75 Ci/g) of ^{18}fluorodeoxyglucose (FDG) tracer solution by tail vein injection, followed by a 0.1 ml saline flush. Dynamic PET imaging for each mouse was immediately performed for 1 h (in vivo PET) using a small animal PET/CT scanner (eXplore Vista; GE Healthcare). The spatial resolution of the PET scanner was 1.6 mm at the centre of the field of view. The data were acquired in 3D mode at the energy window of 250–700 keV, which yields 4% count sensitivity. For each time point, five or six 3D volumes, spanning cortical and subcortical regions, were selected in the centre of the brain, with volumes of 0.2 cm^3 each, and used for quantification using the eXplore Vista software. The averages of these regions were used as the SUV for the animal.

Cell culture. Primary cortical neuronal cultures, derived from E16.5 wild-type C57BL/6J fetuses, were plated in 10% serum-containing neuronal culture medium (neurobasal medium containing B27 supplements, penicillin, streptomycin, and GlutaMax) on either coverslips or culture dishes that were pre-coated with poly-L-ornithine (Sigma p4957). The medium was changed 4 h after initial plating to serum-free neuronal culture medium, and then a half-medium change was performed every three days.

Electroencephalography of *Rest* cKO mice. *Electroencephalogram (EEG) telemetry unit implantation.* Mice were implanted with wireless telemetry units (PhysioTel ETA-F10; Data Sciences International, DSI, St. Paul, MN) under appropriate sterile techniques per laboratory protocol as previously described[33–36]. Mice were anaesthetized by intraperitoneal (i.p.) injection of 100 mg/kg ketamine (Putney Vet, Portland, ME) and 10 mg/kg xylazine (Lloyd Inc., Shenandoah, IA). The transmitter was placed intraperitoneally, and electrodes were threaded subcutaneously to the cranium. After skull exposure, haemostasis, and identification of the cranial sutures, bregma and lambda, two 1-mm diameter burr holes were drilled over the right olfactory bulb (reference) and left occipital cortex (active). The epidural electrodes of the telemetry units, connected to the leads of the transmitter, were placed into the burr holes and secured using stainless steel skull screws. Once in place, the skull screws were covered with dental cement (Dentsply International Inc., Milford, DE). Mice were subcutaneously injected 0 and 24 h post-operatively with 5 mg/kg meloxicam (Norbrook Laboratories, Newry, Northern Ireland) for analgesia. After 1 week of recovery, mice were individually housed in their home cages in a 12 h light–12 h dark, temperature, and humidity controlled chamber with ad libitum access to food and water in preparation for recording.

Video EEG recording, seizure induction and analysis. One-channel video–EEG was recorded differentially between the reference (right olfactory bulb) and active (left occipital lobe) electrodes after 24 h of acclimation in recording chambers. EEG (1,000 Hz), core-body temperature and locomotor activity (200 Hz) signals were continuously sampled over a period of 48 h along with time-registered videos. At the end of baseline EEG acquisition, all mice were provoked with a convulsive dose (40 mg/kg; i.p.) of the GABAA receptor antagonist PTZ (Sigma-Aldrich, Co., St. Louis, MO) to measure seizure susceptibility and evaluate seizure thresholds[33,36]. Mice were continuously monitored for clinical and electrographic epileptiform activity during both periods and this was post hoc verified by blinded review of the video EEG. Following PTZ administration, latency to generalized tonic-clonic seizures (GTCs), number of seizures, and total duration of GTCs were recorded for each mouse. Mice without seizures were assigned a time of 20 min at the end of the PTZ challenge observation period. One *Rest* cKO mouse was excluded from the analysis based on a febrile temperature of 40.68 °C, compared with an average temperature of 34.56 ± 1.48 °C for all other mice.

Immunocytochemical analysis of cultured cells. Embryonic mouse cortical neuronal cultures as described above were plated on poly-L-ornithine-coated coverslips. Stocks of NBQX, APV(Tocris Bioscience Cat. No. 0190, 0106, respectively), and kynurenic acid sodium salt (Abcam, ab146693) were added to neurobasal medium and used in a half-medium change for a final concentration of 5 μM kynurenic acid, 50 μM APV or 2 μM NBQX at day 10 of culture. After 24 h, the culture medium was aspirated and cells were fixed by incubation with 4% (v/v) paraformaldehyde in PBS for 20 min at room temperature, and permeabilized with 0.2% Triton X-100 in PBS for 15 min at room temperature. After a wash in PBS, cells were blocked with 4% BSA in PBS overnight at 4 °C. Primary antibodies were diluted to the appropriate concentration in 4% BSA, and incubated with the cells overnight at 4 °C. Cells were then washed three times in PBST (PBS with 0.05% Triton) for 10 min each, before we added fluorophore-conjugated secondary antibodies for 2 h at room temperature. Fluorophore-labelled cells were then washed in PBST (3 × 10 min) and mounted using Prolong Gold mounting medium with DAPI and anti-fade reagent (Invitrogen). The primary antibodies used in Fig. 5d are rabbit anti-FOXO1 (Cell Signaling 2880) and chicken anti-MAP2 (Sigma-Millipore, AB5392). Nuclei were identified by DAPI labelling, and the cellular distribution of FOXO1 labelling was quantified using Metamorph software. Cell identification parameters were optimized for scoring neuronal cultures, and then the same image analysis macro was applied to all images to generate average FOXO1 cellular intensities in MAP2-positive neurons.

***C. elegans* strains.** The N2 Bristol strain was used as the wild-type background for these studies. *C. elegans* strains were cultured at 20 °C under standard conditions as described[37]. The following mutations and chromosome rearrangements were used: LGI: *spr-4(by105)*[38], *spr-4(tm465)*[15], *daf-16(mu86)*[39], *hT2[bli-4(e937) qIs48] (I;III), unc-13(e51)*[37]; LGIII:*daf-2(e1370)*[39]*eat-4(nj2)*[40]; LGV: *spr-1(ok2144)*[41], *sid-1(pk3321)*[42], *egl-3(gk238)*[43]and LGX *spr-3(ok2525)*[15]; EG7215(oxTi334 [*eft-3p*::*TdTomato*::*h2b*::*unc-54 3′UTR* + *Cbr-unc-119*(+)]). All strains, except for *spr-4(tm465)*, were provided by the Caenorhabditis Genetics Center (CGC), which is funded by the NIH Office of Research Infrastructure Programs (P40 OD010440). Worms that had not been outcrossed previously were outcrossed six times before use. See Supplementary Table 19 for a full listing of strains.

The s*pr-5* mutants exhibited transgenerational effects, including increased defects in DNA double-strand break repair and germline apoptosis[44] as well as lifespan effects[45]. Although we have not fully evaluated the transgenerational phenotypes of *spr-3* and *spr-4* alleles, as a precaution, all lifespan assays were performed with worms no more than five generations removed from a heterozygote ancestor. To facilitate this, *spr-4* alleles were carried over the hT2 balancer described above, while *spr-3*(*ok2525*) was carried over the MosTIC[46] insertion *oxTi335*, which carries a *eft-3*::*tdTomato*::*h2b* fluorescent fusion construct integrated into the X chromosome at 4,348,071 bp. As *spr-3* is located on the X chromosome at 4,514,000 bp, this effectively marked wild-type *spr-3*, allowing us to maintain heterozygous stocks of our double and single mutants.

The *daf-16*::*gfp* fusion line TJ356, bearing transgene *zIs356* [*daf-16p*::*daf-16a/b*::GFP + *rol-6*], was mildly anaesthetized with 0.01% tetramizole and outcrossed to laboratory wild-type males twice, and then mated to *spr-4(by105);spr-3(ok2525)* double mutants. Double mutants bearing *zIs356* were recovered and propagated.

***C. elegans* RNAi.** Feeding RNAi experiments were performed at 20 °C as described[47]. A feeding clone containing a full length *daf-2* cDNA was provided by K. Blackwell. A *daf-16* RNAi vector was provided by E. Greer. Control RNAi was performed by feeding HT115 bacteria carrying the empty pL440 vector. A list of all RNAi clones used is available in Supplementary Table 20.

Enhanced neuronal RNAi was achieved as described[21], by using *sid-1(pk3321)* mutants in which *sid-1* (a dsRNA transporter required for RNAi) is re-expressed solely in neurons via a *punc-119*:*sid-1* transgene. The animals are therefore systemically deficient in RNAi in all cell types except neurons, where RNAi is enhanced by heightened expression of *sid-1*.

Microinjection and transgenic strains. For transgenic *C. elegans* experiments, lines were generated by microinjecting the relevant constructs into the gonads of the indicated worm strains. *Prab-3*::mCherry (pGH8, Addgene: 19359) or *Pmyo-2*::mCherry (pCFJ90, Addgene 19327) were used as coinjection markers. Three independent lines that demonstrated reliable transmission of the marker were propagated as described above for each experiment. Where possible, non-array segregating worms were also maintained as controls. For the dCas9::VP64 experiments, a *peft-3*::*dCas9VP64*::*tbb*-2 UTR construct was cloned using the Wormgate Gateway recombination system into the pCFJ151 MosSCI destination vector. The EG6699 strain, bearing the *ttTi5605*, MosSCI integration site on chromosome II (at 8.42 MB) was raised on HT115 and microinjected as described[48]. Integration was confirmed by genotyping, as well as the absence of unrescued *Unc*$^{-}$ progeny. These worms were then microinjected with a cocktail of four sgRNAs (5 ng/μl each) generated by nested overlap PCR (see Supplementary Table 21 for sequences of sgRNAs), along with a pGH8 *myo-2*::*mcherry* (10 ng/μl) as a marker. Three transgenic lines from independent injections were selected. For simplicity of presentation, these are presented as merged data for lifespans and qPCR validation. For the GCaMP experiment, two of the lines were selected for mating and analysis.

The SPR-4::GFP reporter line was generated by microparticle bombardment using a fusion construct and bombardment protocol as described[49].

Transcript analysis in *C. elegans*. To analyse RNA from transgenic lines, 100 worms (24 h post-L4) of each strain (including controls) were placed into 1.5 ml M9 buffer. For RNA-seq experiments, 450 worms per genotype were grown on FUDR containing plates (starting at L4) and collected in M9, either on day 2 or day 10 of adulthood. Worms were washed once in M9, pelleted by centrifugation, resuspended in 200 μl Trizol, vortexed for 2 min and flash frozen in liquid nitrogen. Worms were then freeze-cracked by thawing in a 37 °C water bath and re-freezing in liquid nitrogen. This was repeated two more times. After the final thaw, 100 μl Trizol was added and the tubes were maintained at room temperature for 5 min. RNA was then extracted with 140 μl chloroform, precipitated with an equal volume of 70% ethanol and transferred to an RNeasy spin column (Qiagen) and purified. Quantitative RT–PCR was performed directly from isolated RNA, using 1 ng of RNA and the Qiagen One Step qPCR mix. All reactions were performed in triplicate. The ddCt method was used to analyse qRT–PCR data, and dCt values were used for statistical analysis.

***C. elegans* motility assay.** Worms were treated for 24 h with the indicated drugs, and then 150 worms were transferred to 1.5 ml liquid nematode growth medium (NGM; 1 mM $MgCl_2$, 1 mM $CaCl_2$, 200 mM KH_2PO_4, 50 mM NaCl) and washed once to remove bacterial clumps. Worms were transferred in 100-μl volumes to a 96 u-shaped-well plate, and assayed in the Nemametrix wMicrotracker (https://nemametrix.com/product-category/phenotyping-products/wmicrotracker/) according to the manufacturer's instructions.

***C. elegans* lifespan determination and stress treatments.** Lifespan and ageing experiments were performed at 20 °C and on fluorodeoxyuridine (FUdR) unless otherwise noted. For each genotype, 20–35 day 1 worms were transferred to NGM plates containing 100 μg/ml FUdR. Worms were scored for viability every day or every other day, and transferred to fresh plates between day 10 and day 14. For *daf-2* mutant worms, worms were moved again at day 20–24. For histamine and ivermectin experiments, where the same plates were used for the entirety of the lifespan, a wetted towel was placed in the container with the plates to mitigate evaporative loss of water from the plates. For lifespan experiments in which untreated worms were transferred to the treatment group (for example, day 8 histamine treatment), control worms with or without treatment were also transferred to fresh plates of the same type to control for any lifespan effects resulting from plate transfer. The presence or absence of FUdR is indicated for each experiment in Supplementary Table 22.

For all lifespans and stress resistance experiments, worms that burst (interior leaking out through the vulva) or bagged (interior hatching of progeny) were discarded from the plate and not used in lifespan analysis, along with animals that crawled off the plate during the course of the assay. Plates with mould or other contamination were discarded.

Quantification of DAF-16::GFP fluorescence. For quantification of GFP fluorescence in fixed animals, 25–30 worms were transferred to an Eppendorf tube containing M9 buffer, washed once in M9 and pelleted. The supernatant was removed and the pellet was frozen in liquid nitrogen. The day before imaging, worm pellets were thawed in PBS with 4% paraformaldehyde (ThermoFisher) and fixed for 30 min at room temperature while rocking. The PFA was removed by washing twice with PBS, with 0.025% Triton (PBST, to prevent sticking), and the worms were stained with DAPI for 10 min at room temperature. The DAPI was removed with a final wash in PBST, and the pellet was resuspended in 15 μl ProLong Gold mounting medium (Life Technologies). The worms were transferred in 12.5 μl mounting medium to a slide, and gently placed under a coverslip, which was then sealed with clear nail polish (Electron Microscopy Sciences).

Slides were imaged on an Olympus Fluoview 1000 confocal microscope, using manufacturer settings for GFP and DAPI (488 nm and 405 nm laser, respectively) within 2 weeks of mounting, and all slides compared with each other were imaged on the same day, in the same imaging session. Worms were imaged via a 40× objective with a 2× digital zoom. For every worm, *Z*-stack image series were taken at 2-μm step sizes (roughly 13–15 images per series). To quantify nuclear GFP levels, these *Z*-stacks were opened in ImageJ (NIH) and flattened using a maximum intensity *Z*-stack projection. For pharyngeal nuclei, three regions of interest (ROI) were selected on the basis of DAPI staining of nuclei, on either side of the pharynx and behind it, encompassing the bulk of the nuclei in that area. These were then used as the ROIs within which to measure GFP fluorescence, using the ImageJ intensity measuring tool. Average scores from the ROIs were computed for each worm. For Extended Data Fig. 6b (middle), Extended Data Fig. 7d (right) and Extended Data Fig. 9a (right), all nuclei located in the middle three *z* planes of the worm were individually selected using the same ROI and intensity measuring tools. These nuclei were then used to calculate an average score per worm.

GCaMP imaging in *C. elegans*. *Data acquisition.* GCaMP imaging was performed in lines bearing *kyIs602* [sra-6::GCaMP3.0, 75 ng/μl + unc-122::GFP, 10 ng/μl], which expresses predominately in the ASH neurons. Worms were removed from plates and mounted on 7.5% agarose pads in liquid NGM (1 mM $MgCl_2$, 1 mM $CaCl_2$, 200 mM KH_2PO_4, 50 mM NaCl), mixed 1:1 with 0.05-μm polystyrene beads (Polysciences, Inc., cat: 08691) as described (http://wbg.wormbook.org/2009/12/01/agarose-immobilization-of-c-elegans/). A coverslip was very gently applied and worms were imaged for a maximum of 30 min after mounting. Videos lasting 144 s (240 frames, ~0.6 frames per second) were recorded on the confocal microscope described above (FV1000), with the confocal aperture widened to 250 μm to allow lower excitation intensity and mitigate *z*-drift. Worms were imaged with factory GFP settings and the 488-nm laser set to 2%. Videos were opened and played in Image J, and excitation events were scored manually for Fig. 4a. Scoring was performed blinded to genotype.

Analysis of GCaMP intensity changes. For analyses of $\Delta F/F_0$ maximum intensity, videos were analysed using a custom MATLAB script, which automatically registered and segmented the ASH neuron and recorded GCaMP fluorescence intensity for each frame. Videos of tracked neurons were manually reviewed and neurons that were poorly tracked were excluded from analysis. To normalize the fluorescence intensity per worm we used $\Delta F/F_0$, calculated as $(F(t) - F_0)/F_0$ where $F(t)$ is the fluorescence intensity at time t and F_0 represents an estimate of the baseline fluorescence, calculated as the 0.2 quantile fluorescence per worm. $\Delta F/F_0$ maximum intensity was the maximum $\Delta F/F_0$ over the entire recording (240 frames). For analysis of nemadipine-treated worms and for worms expressing the HisCl channel (and their controls), ROIs were hand-drawn because the tracking program failed, owing either to low signal intensity (nemadipine treated worms) or the inability to distinguish a confounding GFP signal (HISCL::GFP worms). Some worms were used in multiple GCaMP analyses.

***C. elegans* cloning and genotyping.** The SPR-4::GFP fusion fosmid used in bombardment (Extended Data Fig. 6a, b; Clone: 3167840880351681 C09) was provided by the Transgenome consortium[49]. All primers used for genotyping can be found in Supplementary Table 21.

Human brain gene expression cohorts. *ROSMAP cohort.* Brain samples were from the dorsolateral prefrontal cortex of 638 individuals spanning the range of cognitive function from cognitively normal to MCI to AD from the ROS and MAP cohorts (https://www.synapse.org/#!Synapse:syn3219045).

CommonMind Consortium cohort. Brain samples were from the dorsolateral prefrontal cortex of 602 individuals with schizophrenia or bipolar disease and control individuals with no neuropsychiatric disorders (https://www.synapse.org/#!Synapse:syn2759792).

Gibbs cohort. Brain samples were from the frontal cortex of 146 neurologically normal individuals[11].

RNA library preparation and sequencing. *Human RNA-seq.* Details of RNA-seq for the ROSMAP cohort can be found at https://www.synapse.org/#!Synapse:syn3388564; details of RNA-seq for the CMC can be found at https://www.synapse.org/#!Synapse:syn3157743.

C. elegans *day 2.* Libraries were prepared using Illumina TruSeq Stranded mRNA sample preparation kits from 500 ng of purified total RNA according to the manufacturer's protocol. The finished dsDNA libraries were quantified using Qubit fluorometer, Agilent TapeStation 2200, and RT–qPCR using the Kapa Biosystems library quantification kit according to the manufacturer's protocols. Uniquely indexed libraries were pooled in equimolar ratios and sequenced on an Illumina NextSeq 500 with paired-end 75-bp reads by the Dana-Farber Cancer Institute Molecular Biology Core Facilities.

C. elegans *day 10.* cDNA was synthesized using Clontech SmartSeq v4 reagents from 2 ng RNA, owing to low yields from aged worms. Full-length cDNA was fragmented to a mean size of 150 bp with a Covaris M220 ultrasonicator and Illumina libraries were prepared from 2 ng sheared cDNA using Rubicon Genomics Thruplex DNaseq reagents according to the manufacturer's protocol. The finished dsDNA libraries were quantified using Qubit fluorometer, Agilent TapeStation 2200, and RT–qPCR using the Kapa Biosystems library quantification kit. Uniquely indexed libraries were pooled in equimolar ratios and sequenced on Illumina NextSeq500 run with paired-end 75-bp reads at the Dana-Farber Cancer Institute Molecular Biology Core Facilities. One sequenced sample consisted of primarily ribosomal RNA and was discarded. This sample was reprocessed along with two other previously sequenced samples (as quality controls) with a new library preparation and sequencing. On a principal components plot these three samples showed no clear batch effect compared to the other samples so the resequencing of the sample that was problematic in the original batch was used. The two additional resequenced samples used for quality control were not used in the analysis.

Human sample selection and outlier analysis. *ROSMAP cohort.* Samples were excluded if missing the cognitive diagnosis (cogdx) or post-mortem interval (PMI), if the expression of sex-specific genes did not agree with reported sex, or if RNA integrity (RIN) was less than 6.5. Of the 638 samples with RNA sequencing we removed three because of missing information, 180 because of low RIN, one owing to sex mismatch, and the one remaining sample from sequencing batch 7, the other samples of which had a strong batch effect on principal components plots and were removed because they had low RIN. Next we performed outlier analysis (see below), and removed ten outliers (three no cognitive impairment (NCI), one mild cognitive impairment (MCI), five Alzheimer's disease (AD) dementia, one other dementia). After quality control, 443 individuals remained for analysis (150 NCI, 118 MCI, 164 AD dementia, 11 other dementia).

CommonMind Consortium cohort[10]. We excluded the ten outlier samples identified in the original publication. No other samples were removed. After quality control, of the 602 samples with RNA sequencing, there were 592 individuals for analysis (279 control, 258 schizophrenia, 47 bipolar, 8 affective or mood disorder).

Gibbs cohort. No samples were removed because of missing information or incorrect sex. Next we performed outlier analysis, and removed two outliers. After quality control, there were 144 individuals for analysis.

Outlier analysis. Outlier analysis was performed for each cohort in an iterative manner using only genes expressed in the 'youngold' and 'oldestold' groups at each iteration (see sections Gene expression sample groups for human cohorts and *C. elegans* and Gene expression normalization and covariate adjustment). For the ROSMAP and CMC cohorts we used edgeR TMM-normalized log(counts per million (CPM)) expression. For the Gibbs cohort we used $\log_2$ expression. At each iteration, the sample deemed to be the strongest outlier, if any, was removed and the process was iterated until no outliers were detected. Outlier detection was performed using principal components analysis, agglomerative hierarchical clustering using the Euclidean distance metric and average linkage criterion, and pairwise correlation of gene expression per sample. Samples were classified as outliers if they were isolated on a plot of the first and second principal components or in the hierarchical clustering tree, and had relatively low correlation with other samples determined as its mean pairwise correlation with other samples more than 3 s.d. below the mean.

RNA sequencing read alignment and quantification of gene expression. *ROSMAP cohort.* BAM files containing reads aligned to hg19 were obtained from synapse (https://www.synapse.org/#!Synapse:syn3388564). Reads were obtained from these BAM files using Picard v1.138 (http://broadinstitute.github.io/picard/) SamToFastq. Reads were aligned to GRCh38 with Ensembl GRCh38.86 gene models using STAR version 2.5.2b[50] with options–outFilterMismatchNoverLmax 0.04 –outFilterMismatchNmax 999 –alignSJDBoverhangMin 1 –alignSJoverhangMin 8 –outFilterMultimapNmax 20 –outFilterType BySJout –alignIntronMin 20 –alignIntronMax 1000000 –alignMatesGapMax 1000000. The expression of genes was quantified as gene counts using FeatureCounts v1.5.1[51] with options -C -p -B -s 2 -t exon -g gene_id.

CommonMind Consortium cohort. Gene counts were obtained from synapse (https://www.synapse.org/#!Synapse:syn3346749).

C. elegans *day 2 and day 10.* Quality control of sequencing reads was performed with FastQC (https://www.bioinformatics.babraham.ac.uk/projects/fastqc/). Reads were aligned to the *C. elegans* WBcel235 genome with Ensembl WBcel235.86 gene models using STAR version 2.5.2b with options –outFilterMismatchNoverLmax 0.04 –outFilterMismatchNmax 999 –alignSJDBoverhangMin 1 –alignSJoverhangMin 8 –outFilterMultimapNmax 20 –outFilterType BySJout –alignIntronMin 15 –alignIntronMax 1000000 –alignMatesGapMax 1000000. The expression of genes was quantified as gene counts using FeatureCounts v1.5.1 with options -C -p -B -s 2 -t exon -g gene_id for day 2 and -C -p -B -s 0 -t exon -g gene_id for day 10. Data are available in the Gene Expression Omnibus (GEO) under accession number GSE123146.

Gene expression sample groups for human cohorts and *C. elegans*. *ROSMAP cohort.* ROSMAP was our discovery cohort. On the basis of hierarchical clustering of age-associated genes (see section Hierarchical clustering to select age group cutoffs), we partitioned individuals with no cognitive impairment into the age groups: youngold (28 individuals, ages ≥70 and ≤80 years), middleold (33 individuals, ages >80 and <85 years), and oldestold (89 individuals, ages 85–101 years). Individuals with cognitive impairment were grouped into a separate cognitive impairment group (293 individuals).

CommonMind Consortium cohort. The CMC cohort was a replication cohort for the ROSMAP results. We partitioned control individuals into four age groups: young (105 individuals, ages ≥17 and ≤60 years), youngold (96 individuals, ages ≥60 and ≤80 years), middleold (19 individuals, ages >80 and <85 years) and oldestold (59 individuals, ages ≥85 and 90+ years; in this cohort, age of death greater than 90 years was censored to 90+). Individuals with neuropsychiatric illnesses were grouped into a separate group (313 individuals).

Gibbs cohort. The Gibbs cohort was a replication cohort for the ROSMAP results. We partitioned cognitively normal individuals into four age groups: young (104 individuals, ages ≥15 and <55 years), youngold (18 individuals, ages ≥55 and ≤80 years), middleold (3 individuals, ages >80 and <85 years), and oldestold (19 individuals, ages 85–101 years).

Throughout the paper, 'individuals with extended longevity' refers to individuals in the oldestold groups defined above.

C. elegans *day 2 and day 10.* There were four genotypes of worm: *daf-2*, *daf-2; spr-4;spr-3*, N2, and *spr-4;spr-3*, and each genotype had three biological replicates. Each genotype was considered as a separate group for analysis.

Gene expression normalization and covariate adjustment. *ROSMAP cohort.* Gene counts were input to edgeR[52]. Genes were deemed to be expressed if $\geq$10 individuals in a combined youngold and oldestold group had $\geq$1 CPM. Genes not satisfying these criteria were removed, keeping the original library sizes. These were expressed genes used during each iteration of outlier analysis. After outlier analysis, this filtering retained 18,511 expressed genes out of 58,051 annotated genes for analyses involving the ROSMAP cohort. Counts were then normalized using the TMM method in edgeR. Finally, log(CPM) values were calculated for analyses other than differential expression.

To adjust gene expression for covariates we fit the linear regression model for each gene separately using lm() in R: gene expression ~ group + covariates where gene expression is log(CPM), and using the group and covariates for ROSMAP. For ROSMAP, group was a factor with four levels: youngold, middleold, oldestold, and cognitivedecline, with cognitivedecline as the reference level. The covariates were sex (factor, two levels), RIN (continuous), RIN^2 (continuous), PMI (continuous), and sequencing batch (factor, eight levels). The final normalized and adjusted gene expression values were derived from adding the regression residuals to the estimated effect of the group level to preserve the effect of the group on expression. These normalized and adjusted gene expression values were used to perform gene–gene regression analysis and gene–gene group regression analysis, and to visualize gene expression.

CommonMind Consortium cohort. Gene counts were input to edgeR. Genes were deemed expressed if $\geq$10 individuals in a combined youngold and oldestold group had $\geq$1 CPM. Genes that did not satisfy these criteria were removed, maintaining the original library sizes. These were expressed genes used during each iteration of outlier analysis. After outlier analysis, this filtering retained 19,453 expressed genes out of 56,632 annotated genes for analyses involving the CMC cohort. Counts were then normalized using the TMM method in edgeR. Finally, log(CPM) values were calculated for analyses other than differential expression. To adjust gene expression for covariates, we fit the linear regression model for each gene separately using lm() in R: gene expression ~ group + covariates where gene expression is log(CPM), and using the group and covariates for CMC. For CMC, group was a factor with five levels: young, youngold, middleold, oldestold, and neuropsychiatric illness, with neuropsychiatric illness as the reference level. The covariates used were selected from those used in the original publication: sex (factor, two levels), RIN (continuous), RIN^2 (continuous), PMI (continuous), clustered batch (factor, nine levels), and institute (factor, three levels). The final normalized and adjusted gene expression values were derived by adding the regression residuals to the estimated effect of the group level to preserve the effect of the group on expression. These normalized and adjusted gene expression values were used to perform gene–gene regression analysis and gene–gene group regression analysis, and to visualize gene expression.

Gibbs cohort. Gene expression data measured on the Illumina humanRef-8 v2.0 expression beadchip platform were downloaded from NCBI GEO GSE15745. Raw intensity values for each probe were transformed using the rank invariant normalization method by the authors[11], and then $\log_2$ transformed for analysis. Probes were deemed expressed if $\geq$10 individuals in a combined youngold and oldestold group had detection $P < 0.01$. Unmapped probes according to updated GEO Platform (GPL) annotation were removed. These were expressed probes used during each iteration of outlier analysis. After outlier analysis, this filtering retained 13,239 expressed probes out of 22,184 probes for analyses involving the Gibbs cohort.

To adjust gene expression for covariates we fit the linear regression model for each gene separately using lm() in R: probe expression ~ group + covariates where probe expression is $\log_2$ expression, and using the group and covariates for Gibbs. For Gibbs, group was a factor with four levels: young, youngold, middleold, and oldestold, with young as the reference level. The covariates were sex (factor, two levels), PMI (continuous), and prep hybridization batch (factor, seven levels). The final normalized and adjusted probe expression values were derived by adding the regression residuals to the estimated effect of the group level to preserve the effect of the group on expression. These normalized and adjusted probe expression values were used to visualize probe expression.

C. elegans *day 2 and day 10.* Gene counts were input to edgeR. Genes were deemed expressed if $\geq$3 samples had $\geq$1 CPM. Genes not satisfying these criteria were removed, keeping the original library sizes. This filtering retained 12,981 expressed genes out of 46,739 annotated genes for analyses involving *C. elegans* day 2 and 15,154 expressed genes for analyses involving *C. elegans* day 10. Counts were then normalized using the TMM method in edgeR. Finally, log(CPM) values were calculated for analyses other than differential expression. For day 2, covariate adjustment was not necessary because there were no other covariates beyond the group variable. For day 10 we did not include a batch covariate because there was no observed batch effect on a principal components plot, and results were similar if a batch covariate was included and the two dropped technical repeat sequencings were used instead of their original sequenced reads (data not shown). Thus, covariate adjustment was not necessary because there were no other covariates beyond the group variable. These normalized gene expression values were used to visualize gene expression.

To visualize differentially expressed genes in heat maps, normalized gene expression values were transformed to a z-score per gene and thresholded to $[-3, 3]$.

Differential expression analysis. *ROSMAP cohort.* Differential expression analysis between the oldestold and youngold groups with covariate adjustment using the covariates listed above for ROSMAP was performed for expressed genes using edgeR (estimateDisp, glmFit, and glmLRT with default arguments) in R. All 443 samples were included to increase statistical power during covariate modelling. Genes were considered differentially expressed if the Benjamini and Hochberg false discovery rate (FDR) was $\leq$0.1, which was calculated using the R function p.adjust with argument method = 'fdr'[53].

CommonMind Consortium cohort. Differential expression analysis between the oldestold and youngold groups with covariate adjustment using the covariates listed above for the CMC was performed for expressed genes using edgeR (estimateDisp, glmFit, and glmLRT with default arguments) in R. All 592 samples were included to increase statistical power during covariate modelling. Genes were considered differentially expressed if FDR $\leq$ 0.05 and the absolute value of the fold change was $\geq$1.2.

Gibbs cohort. Differential expression analysis between the oldestold and youngold groups with covariate adjustment using the covariates listed above for Gibbs was performed for expressed probes using linear regression models in limma (lmFit and eBayes with default arguments) in R. All 144 samples were included to increase statistical power during covariate modelling. Probes were considered differentially expressed if FDR $\leq$ 0.05.

C. elegans *day 2 and day 10.* Differential expression analysis between all pairs of groups such as *spr-4;3;daf-2* versus *daf-2* was performed for expressed genes using edgeR (estimateDisp, glmFit, and glmLRT with default arguments) in R. All 12 samples were included during edgeR analysis. Genes were considered differentially expressed if FDR $\leq$ 0.05.

Gene sets and gene set enrichment analysis. Gene annotation and gene sets used for functional gene classification into biological process (BP), molecular function (MF), and cellular component (CC) were from the GRCh38.p7 database downloaded from Ensembl Biomart (https://www.ensembl.org/biomart/martview/) on November 2, 2016.

Synaptic transmission genes were genes that had direct or indirect annotation for the GO biological process 'Chemical synaptic transmission' (GO: 0007268).

To identify REST target genes, the REST RE1 motif position-specific weight matrix MA0138.2 was obtained from JASPAR[54]. FIMO version 4.10.1[55] was used with the *Homo sapiens* genome sequence GRCh38 to predict REST binding sites. A gene was defined to be a REST target if it had an RE1 motif with motif $P < 1 \times 10^{-7}$ that was $\pm$10 kb from the transcription start site of any transcript of the gene in the Ensembl GRCh38.86 gene models. This procedure identified 2,632 REST target genes before filtering for expressed genes in each cohort during gene set enrichment analysis.

ENCODE ChIP–seq transcription factor target gene sets were from the ENCODE_TF_ChIP-seq_2015 database[56] downloaded from http://amp.pharm.mssm.edu/Enrichr/ on 8 March 2018.

Cell type analysis gene sets were derived from a transcriptome database of the major cell classes of the mouse cerebral cortex[57] using data from https://web.stanford.edu/group/barres_lab/brain_rnaseq.html. To select cell marker genes, first we calculated the fold expression of each gene in each cell type by dividing the fragments per kilobase of transcript per million mapped reads (FPKM) expression in that cell type by the mean of the FPKM expression in the other six cell types. For each cell type we selected as cell marker genes those that had at least tenfold higher expression in that cell type and that had one-to-one human–mouse homologues. Homologues were downloaded from http://www.informatics.jax.org/downloads/reports/HOM_MouseHumanSequence.rpt on November 16, 2016.

DAF-16 class I (upregulated) genes were derived by selecting genes with FDR < 0.01 and class == 'up' from Supplementary Table 1 of Tepper et al.[58].

For gene set enrichment analysis of differentially expressed genes, we retained only genes in each gene set that were expressed in that differential expression analysis. Gene set enrichment analysis was performed separately for upregulated genes and non-upregulated genes, downregulated genes and non-downregulated genes, and differentially regulated genes and non-differentially regulated genes. For Gene Ontology gene sets, gene set enrichment was determined using the topGO R package[59] using the classic algorithm and Fisher's statistic. Gene set enrichment for REST target genes, ENCODE ChIP–seq transcription factor target gene sets, and cell type analysis gene sets was performed using the hypergeometric distribution

(one-tailed). Gene sets with fewer than five genes after filtering for expressed genes were removed before the gene set enrichment false discovery rates were calculated.

To calculate the statistics for overlap of *daf-2* upregulated genes, *spr-4;spr-3;daf-2* upregulated genes, *spr-4;spr-3;daf-2* downregulated genes, and *daf-16* class I genes for *C. elegans* day 10 we used the SuperExactTest version 1.0.0 R package[60].

For meta-analysis of GO terms and ENCODE ChIP–seq transcription factor target gene set enrichment from the ROSMAP, CMC, and Gibbs cohorts, we used Stouffer's method with weights[61] for combining *P* values implemented in the sumz function in the metap R package[62]. *P* values equal to 1 were replaced with 0.999999 to comply with the requirement that $0 < P < 1$. For study weights we used the square root of the total number of individuals in the combined youngold and oldestold group for each study (ROSMAP, sqrt(117); CMC, sqrt(155); Gibbs, sqrt(37))[61].

Hierarchical clustering to select age group cutoffs. Normalized and adjusted gene expression values were derived as described in the section Gene expression normalization and covariate adjustment, with the following changes. First, the group variable was a factor with levels cogdx1, cogdx2, cogdx3, cogdx4, cogdx5, and cogdx6 (ROSMAP); control, schizophrena, bipolar, affective (CMC); or not included (Gibbs). Next, genes were deemed expressed if ≥10 individuals in the cognitively normal group (ROSMAP, cogdx1; CMC, control with age ≥ 60) had more than 1 CPM. Genes not satisfying these criteria were removed, keeping the original library sizes. For the Gibbs cohort, probes were deemed expressed if ≥10 individuals with age ≥ 55 had detection $P < 0.01$ and no samples had NA values. Probes not satisfying these criteria were removed. These were expressed genes used for analysis. This filtering retained: ROSMAP, 18,734 expressed genes; CMC, 19,615 expressed genes; Gibbs, 13,411 expressed probes. For RNA-seq data, counts were then normalized using the TMM method in edgeR, and log(CPM) values were calculated for expression. Finally, age was included as a continuous covariate, and the effects of group and age were added back to the residuals. Then cognitively normal aged individuals were selected in each cohort (ROSMAP, cogdx1; CMC, control with age ≥ 60; Gibbs, age ≥ 55). To determine age-associated genes, the expression of each expressed gene was correlated with the age of death of the individual using Spearman's correlation. Genes with Spearman rank correlation FDR < 0.1 (ROSMAP, $n = 1{,}025$ genes) or FDR < 0.05 (CMC, $n = 6{,}828$ genes; Gibbs, $n = 203$ probes) were age-associated genes. Permuting sample ages before calculating the Spearman correlations gave no genes that passed the FDR threshold. Genes were then normalized to have mean 0 and s.d. 1 across individuals, and genes with normalized expression ≥3 or ≤−3 were set to 3 or −3, respectively. The Pearson correlation coefficient between individuals was then calculated using only age-associated genes.

Agglomerative hierarchical clustering using the Euclidean distance metric and average linkage criterion was performed on the matrix of pair-wise Pearson correlations to cluster individuals. The resulting tree was cut into three groups, and the distribution of the age of death of individuals of each group was analysed. Using the ROSMAP cohort, for the cluster with the smallest median age, with c1 individuals, we calculated the number of individuals, nyoc, with age of death in [70, youb], of nyo total, and for the cluster with the largest median age, of c2 individuals, we calculated the number of individuals, nooc, with age of death in [oolb, Inf), of noo total, as the age boundaries youb and oolb varied. For each set of age cutoffs we assigned a score as $(\text{nyoc/nyo} \times c1 + \text{nooc/noo} \times c2)/(c1 + c2)$. To ensure adequate sample sizes for differential expression and because individuals with older ages appeared more heterogeneous in the cluster heat map, we considered only age cutoffs with at least 25 individuals in the youngold group and at least 75 individuals in oldestold group. On the basis of the top scoring age cutoffs in the ROSMAP cohort, we selected youb = 80 and oolb = 85. Thus, the age cutoffs for defining the youngold, middleold, and oldestold groups used for differential expression in the ROSMAP, CMC, and Gibbs cohorts were selected to be ≤80, >80 and <85, and ≥85, respectively.

Statistical analysis and data representation. Statistical analysis was performed using R. Statistical tests used are noted in the figure legends or in the relevant Methods section. Throughout the paper, all tests are two-sided and unpaired unless stated otherwise. A significance level of 0.05 was used to reject the null hypothesis unless stated otherwise.

Box plots throughout the paper show the median, lower and upper hinges (first and third quartiles), upper whisker (hinge to the largest value no further than 1.5 × IQR from the hinge), lower whisker (hinge to the smallest value at most 1.5 × IQR from the hinge), and outlying points beyond the whiskers. Additionally, all points are plotted on top of the box plot and randomly jittered horizontally

A *t*-test was used for parametric comparisons between two groups with normally distributed data, and used t.test(). For groups with equal variance, Student's *t*-test was used (argument var.equal = TRUE); otherwise Welch's *t*-test was used (argument var.equal = FALSE). ANOVA was used for parametric comparisons between more than two groups and used aov(). The Mann–Whitney *U*-test was used for nonparametric comparisons between two groups without knowledge of their distribution and used wilcox.test() with arguments exact = TRUE, correct = FALSE. Levene's test was used to investigate the homogeneity of variance across groups and used leveneTest() from the 'car' R package. *Q*–*Q* plots and the Shapiro–Wilk test were used to assess normality and used shapiro.test(). The Bonferroni outlier test was used to assess outliers and used outlierTest() from the 'car' R package. The log-rank test was used to compare the survival distributions of two groups. Survival statistics were calculated using survfit() with argument type = 'kaplan-meier' and survdiff(). To determine whether there was a linear relationship between two variables we fit a linear regression model and tested the null hypothesis that the slope of the regression line is 0 using a two-sided *t*-test using lm(). *P* values were corrected for multiple comparisons where noted using p.adjust() with argument method = 'fdr', 'holm', or 'bonferroni' for false discovery rate, Holm's method, or Bonferroni correction, respectively. The GCaMP imaging data indicated that nonparametric analyses were most appropriate and thus were used for all GCaMP analyses. In Fig. 2e, the presence of candidate outliers and/or potential non-normality for time points 1–12.5 min suggested that a Mann–Whitney *U*-test was more appropriate although a *t*-test produced similar conclusions. Meta-analysis of lifespan experiments that performed pairwise comparisons among more than two groups (Extended Data Fig. 8a right, Extended Data Fig. 8c) used pairwise Student's *t*-tests implemented in pairwise.t.test() with argument pool.sd = TRUE to calculate a common s.d. used for all groups and comparisons.

Reporting summary. Further information on research design is available in the Nature Research Reporting Summary linked to this paper.

Data availability

Data from the ROSMAP cohort are available under controlled use conditions set by human privacy regulations. To access the data, a data use agreement is needed. This registration is in place solely to ensure the anonymity of the ROSMAP study participants. Data can be requested on the Rush Alzheimer's Disease Center Resource Sharing Hub at http://www.radc.rush.edu/. *C. elegans* RNA-seq data are available in the Gene Expression Omnibus (GEO) under accession number GSE123146.

Code availability

All code used in the analysis of data presented in this manuscript is available upon request.

29. Bennett, D. A., Schneider, J. A., Arvanitakis, Z. & Wilson, R. S. Overview and findings from the religious orders study. *Curr. Alzheimer Res.* **9**, 628–645 (2012).
30. Bennett, D. A. et al. Overview and findings from the Rush Memory and Aging Project. *Curr. Alzheimer Res.* **9**, 646–663 (2012).
31. Mu, X. et al. A gene network downstream of transcription factor Math5 regulates retinal progenitor cell competence and ganglion cell fate. *Dev. Biol.* **280**, 467–481 (2005).
32. Mao, C. A. et al. Neuronal transcriptional repressor REST suppresses an Atoh7-independent program for initiating retinal ganglion cell development. *Dev. Biol.* **349**, 90–99 (2011).
33. Dhamne, S. C. et al. Replicable in vivo physiological and behavioral phenotypes of the *Shank3B* null mutant mouse model of autism. *Mol. Autism* **8**, 26 (2017).
34. Kelly, E. et al. mGluR5 modulation of behavioral and epileptic phenotypes in a mouse model of tuberous sclerosis complex. *Neuropsychopharmacology* **43**, 1457–1465 (2018).
35. Purtell, H. et al. Electrographic spikes are common in wildtype mice. *Epilepsy Behav.* **89**, 94–98 (2018).
36. Yuskaitis, C. J. et al. A mouse model of DEPDC5-related epilepsy: neuronal loss of Depdc5 causes dysplastic and ectopic neurons, increased mTOR signaling, and seizure susceptibility. *Neurobiol. Dis.* **111**, 91–101 (2018).
37. Brenner, S. The genetics of *Caenorhabditis elegans*. *Genetics* **77**, 71–94 (1974).
38. Lakowski, B. et al. Two suppressors of sel-12 encode C2H2 zinc-finger proteins that regulate presenilin transcription in *Caenorhabditis elegans*. *Development* **130**, 2117–2128 (2003).
39. Kenyon, C., Chang, J., Gensch, E., Rudner, A. & Tabtiang, R. A *C. elegans* mutant that lives twice as long as wild type. *Nature* **366**, 461–464 (1993).
40. Ohnishi, N., Kuhara, A., Nakamura, F., Okochi, Y. & Mori, I. Bidirectional regulation of thermotaxis by glutamate transmissions in *Caenorhabditis elegans*. *EMBO J.* **30**, 1376–1388 (2011).
41. Jarriault, S. & Greenwald, I. Suppressors of the egg-laying defective phenotype of *sel-12* presenilin mutants implicate the CoREST corepressor complex in LIN-12/Notch signaling in *C. elegans*. *Genes Dev.* **16**, 2713–2728 (2002).
42. Winston, W. M., Molodowitch, C. & Hunter, C. P. Systemic RNAi in *C. elegans* requires the putative transmembrane protein SID-1. *Science* **295**, 2456–2459 (2002).
43. *C. elegans* Deletion Mutant Consortium. Large-scale screening for targeted knockouts in the *Caenorhabditis elegans* genome. *G3 (Bethesda)* **2**, 1415–1425 (2012).
44. Nottke, A. C. et al. SPR-5 is a histone H3K4 demethylase with a role in meiotic double-strand break repair. *Proc. Natl Acad. Sci. USA* **108**, 12805–12810 (2011).
45. Greer, E. L., Becker, B., Latza, C., Antebi, A. & Shi, Y. Mutation of *C. elegans* demethylase spr-5 extends transgenerational longevity. *Cell Res.* **26**, 229–238 (2016).

46. Robert, V. J., Katic, I. & Bessereau, J. L. Mos1 transposition as a tool to engineer the *Caenorhabditis elegans* genome by homologous recombination. *Methods* **49**, 263–269 (2009).
47. Kamath, R. S. & Ahringer, J. Genome-wide RNAi screening in *Caenorhabditis elegans*. *Methods* **30**, 313–321 (2003).
48. Frøkjær-Jensen, C., Davis, M. W., Ailion, M. & Jorgensen, E. M. Improved Mos1-mediated transgenesis in *C. elegans*. *Nat. Methods* **9**, 117–118 (2012).
49. Sarov, M. et al. A genome-scale resource for in vivo tag-based protein function exploration in *C. elegans*. *Cell* **150**, 855–866 (2012).
50. Dobin, A. et al. STAR: ultrafast universal RNA-seq aligner. *Bioinformatics* **29**, 15–21 (2013).
51. Liao, Y., Smyth, G. K. & Shi, W. featureCounts: an efficient general purpose program for assigning sequence reads to genomic features. *Bioinformatics* **30**, 923–930 (2014).
52. Robinson, M. D., McCarthy, D. J. & Smyth, G. K. edgeR: a Bioconductor package for differential expression analysis of digital gene expression data. *Bioinformatics* **26**, 139–140 (2010).
53. Benjamini, Y. & Hochberg, Y. Controlling the false discovery rate: a practical and powerful approach to multiple testing. *J. R. Stat. Soc. B* **57**, 289–300 (1995).
54. Sandelin, A., Alkema, W., Engström, P., Wasserman, W. W. & Lenhard, B. JASPAR: an open-access database for eukaryotic transcription factor binding profiles. *Nucleic Acids Res.* **32**, D91–D94 (2004).
55. Grant, C. E., Bailey, T. L. & Noble, W. S. FIMO: scanning for occurrences of a given motif. *Bioinformatics* **27**, 1017–1018 (2011).
56. Chen, E. Y. et al. Enrichr: interactive and collaborative HTML5 gene list enrichment analysis tool. *BMC Bioinformatics* **14**, 128 (2013).
57. Zhang, Y. et al. An RNA-sequencing transcriptome and splicing database of glia, neurons, and vascular cells of the cerebral cortex. *J. Neurosci.* **34**, 11929–11947 (2014).
58. Tepper, R. G. et al. PQM-1 complements DAF-16 as a key transcriptional regulator of DAF-2-mediated development and longevity. *Cell* **154**, 676–690 (2013).
59. Alexa, A. & Rahnenfuhrer, J. topGO: enrichment analysis for gene ontology. *R package version* **2340** (2018).
60. Wang, M., Zhao, Y. & Zhang, B. Efficient test and visualization of multi-set intersections. *Sci. Rep.* **5**, 16923 (2015).
61. Zaykin, D. V. Optimally weighted Z-test is a powerful method for combining probabilities in meta-analysis. *J. Evol. Biol.* **24**, 1836–1841 (2011).
62. Dewey, M. Metap: meta analysis of significance values. R package Version 10 (2018).

Acknowledgements We thank members of the Yankner laboratory for suggestions and discussion, and the Hsieh laboratory for providing the anti-mouse REST antibody. This work was supported by an NIH Director's Pioneer Award (DP1OD006849) and NIH grants RO1AG046174 and RO1AG26651 to B.A.Y., RO1GM072551 to M.P.C., P30AG10161, R01AG15819, R01AG17917, R01AG36836 and U01AG46152 to D.A.B., EY024376 to C.-A.M., EY011930 to W.H.K. and K99AG050830 to J.M.Z., and grants from the Glenn Foundation for Medical Research and The Ludwig Family Foundation to B.A.Y. Data were generated as part of the CMC, supported by funding from Takeda Pharmaceuticals Company Limited, F. Hoffman-La Roche Ltd and NIH grants R01MH085542, R01MH093725, P50MH066392, P50MH080405, R01MH097276, RO1-MH-075916, P50M096891, P50MH084053S1, R37MH057881, R37MH057881S1, HHSN271201300031C, AG02219, AG05138 and MH06692.

Author contributions J.M.Z., P.O. and N.D. performed experiments in *C. elegans*; D.D. performed statistical analysis and informatics on human brain and *C. elegans* RNA-seq; L.A. and D.D. analysed *Rest* cKO mice and human brain sections; L.A., S.C.D. and A.R. performed PET–CT and electrophysiological analysis of mice; J.M.Z. performed cell culture; C.-A.M., W.H.K. and G.M.C. contributed reagents; D.A.B. contributed brain samples and data from the ROSMAP cohort; J.M.Z., D.D., M.P.C. and B.A.Y. contributed to the overall study design; B.A.Y. directed the study; and B.A.Y., J.M.Z. and D.D. wrote the manuscript, which was examined by all authors.

Competing interests G.M.C. is a cofounder and senior advisor for GC Therapeutics, Inc, which uses transcription factors for therapeutics. The other authors declare no competing interests.

Additional information

Supplementary information is available for this paper at https://doi.org/10.1038/s41586-019-1647-8.

Correspondence and requests for materials should be addressed to B.A.Y.

Peer review information *Nature* thanks Nektarios Tavernarakis and the other, anonymous, reviewer(s) for their contribution to the peer review of this work.

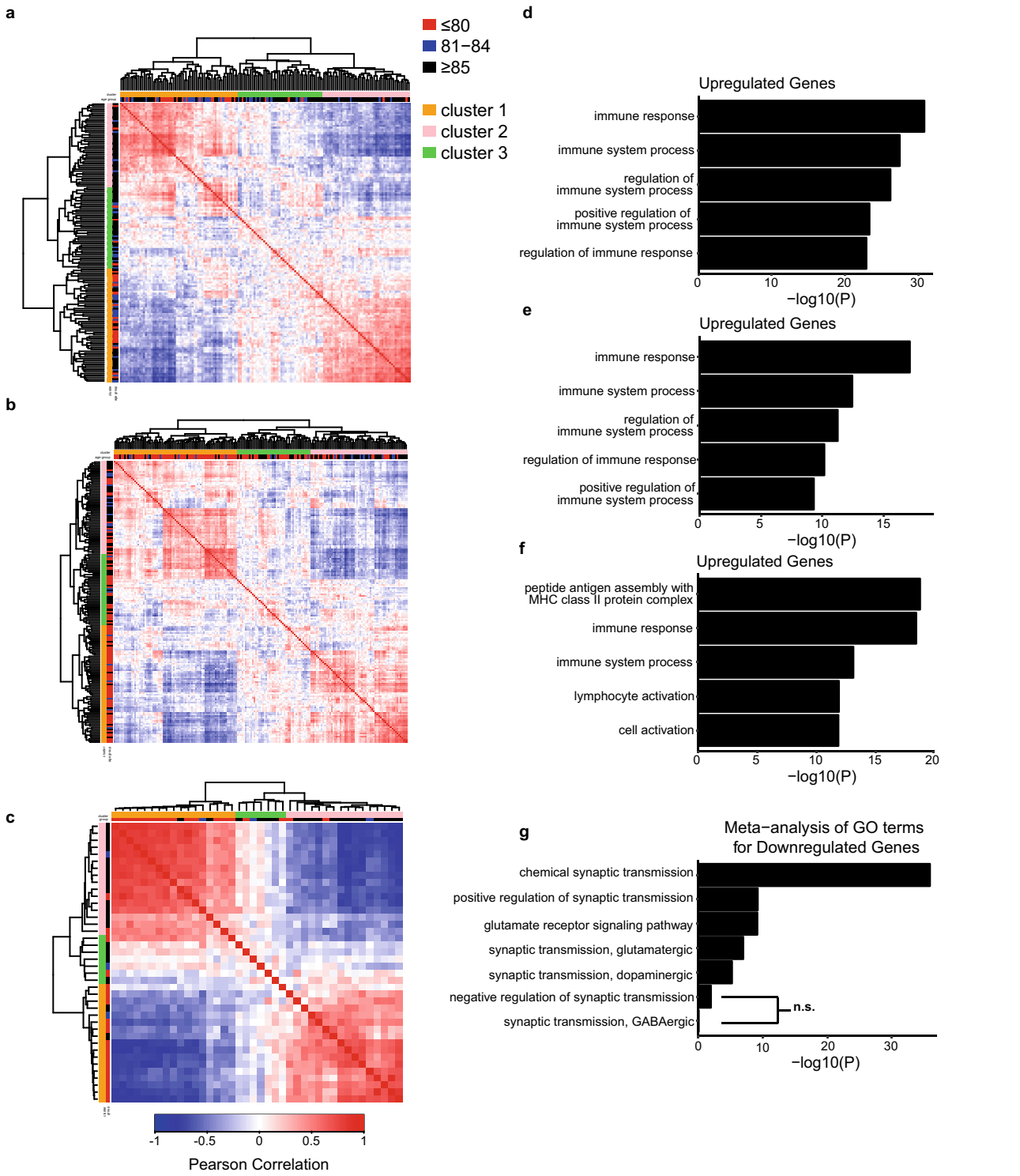

Extended Data Fig. 1 | Partitioning of the ageing human population for analysis of gene expression in the brain. a–c, Adjusted gene expression profiles of age-associated genes were compared between cognitively normal aged individuals to derive a matrix of Pearson correlation coefficients that indicate the degree of similarity between any two cases in the ROSMAP (**a**, dorsolateral prefrontal cortex, $n = 150$ individuals), CMC (**b**, dorsolateral prefrontal cortex, $n = 174$ individuals) and Gibbs (**c**, frontal cortex, $n = 40$ individuals) cohorts. **d–f**, Most significantly enriched GO terms for upregulated genes in the cortex of cognitively normal individuals who lived to be ≥85 years old relative to individuals who lived to be ≤80 years old in the ROSMAP (**d**, $n = 117$ individuals), CMC (**e**, $n = 155$ individuals), and Gibbs (**f**, $n = 37$ individuals) cohorts. *P* values were calculated using Fisher's exact test (see Methods). **g**, Meta-analysis of GO term enrichment for downregulated genes. Shown are selected GO terms related to excitatory and inhibitory synaptic transmission. The individual cohort enrichment *P* values were combined using Stouffer's method (see Methods). NS, not significant (FDR > 0.1).

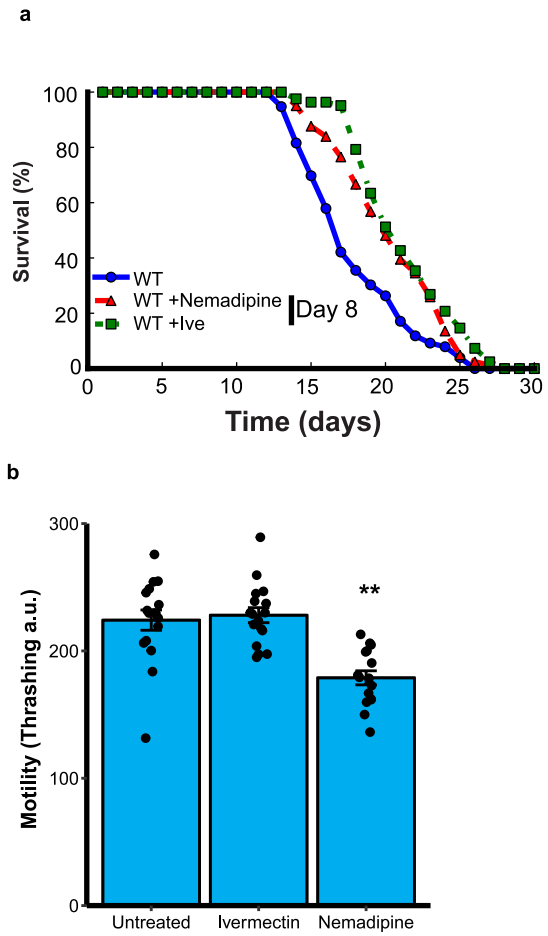

Extended Data Fig. 2 | Ivermectin and nemadipine extend lifespan without interfering with worm motility. a, Worms were transferred at day 8 to either standard NGM plates or plates containing ivermectin (Ive, 1 pg ml^{-1}) or nemadipine (2 μM). Shown is a representative curve of an experiment repeated twice. Nemadipine versus wild-type, $P = 3.2 \times 10^{-4}$; ivermectin versus wild-type, $P = 2.2 \times 10^{-7}$ by log-rank test. Nemadipine, $n = 81$; ivermectin, $n = 82$; wild-type, $n = 76$. **b**, Day 2 worms treated with nemadipine or ivermectin for 24 h were transferred to liquid culture and thrashing rate was assessed using the Nemametrix wMicrotracker (see Methods). Shown are mean motility scores for the first 60 min ± s.e.m. Untreated, $n = 17$ wells; ivermectin, $n = 17$ wells; nemadipine, $n = 16$ wells. Each well contained about 10 worms. $^{**}P = 1.7 \times 10^{-4}$ versus untreated, Mann–Whitney U-test with multiple testing correction by Holm's method. Results are representative of an experiment replicated twice.

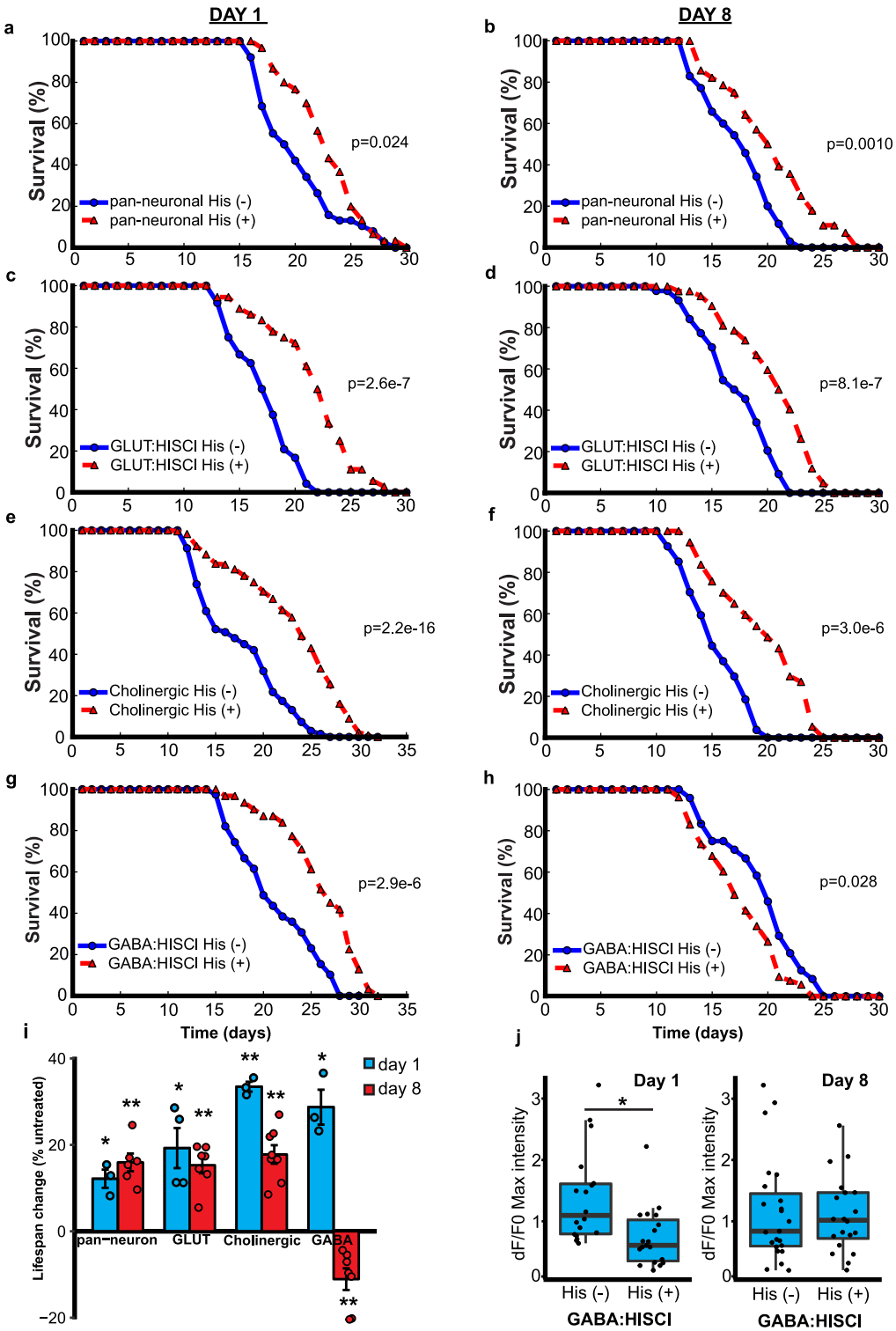

Extended Data Fig. 3 | Repression of multiple neurotransmitter systems extends lifespan in *C. elegans*. **a**–**h**, *C. elegans* lines expressing the transgenic HisCl1 channel in the indicated neuronal populations were treated with 10 mM histamine (His+) starting at adult day 1 (**a**, **c**, **e**, **g**) or day 8 (**b**, **d**, **f**, **h**) and compared to untreated controls (His–). *P* values calculated by log-rank test. See Supplementary Table 22 for individual *n* values and statistics. **i**, Mean lifespan extension ± s.e.m. for worms treated with histamine at days 1 or 8 relative to untreated controls for at least three independent replicates. $*P < 0.05$, $**P < 0.01$ by Student's *t*-test. HisCl1was driven using the GAL4SK:VP64 system for the GABAergic (GABA), glutamatergic (GLUT) and cholinergic systems, using *unc-47*, *eat-4*, and *unc-17* drivers, respectively (see Supplementary Table 19). **j**, Reduced ASH neuron excitation following inhibition of GABA activity at day 1 but not day 8. Shown is normalized maximum GCaMP fluorescence in day 1 and 8 *unc-47*:HisCl1 worms that were treated with 10 mM histamine (His (+)) on the indicated day, or untreated controls (His (–)). Day 1 His(–), $n = 18$ worms; day 1 His(+), $n = 19$ worms; day 8 His(–), $n = 23$ worms; day 8 His(+), $n = 20$ worms. $*P = 1.1 \times 10^{-3}$ by Mann–Whitney *U*-test.

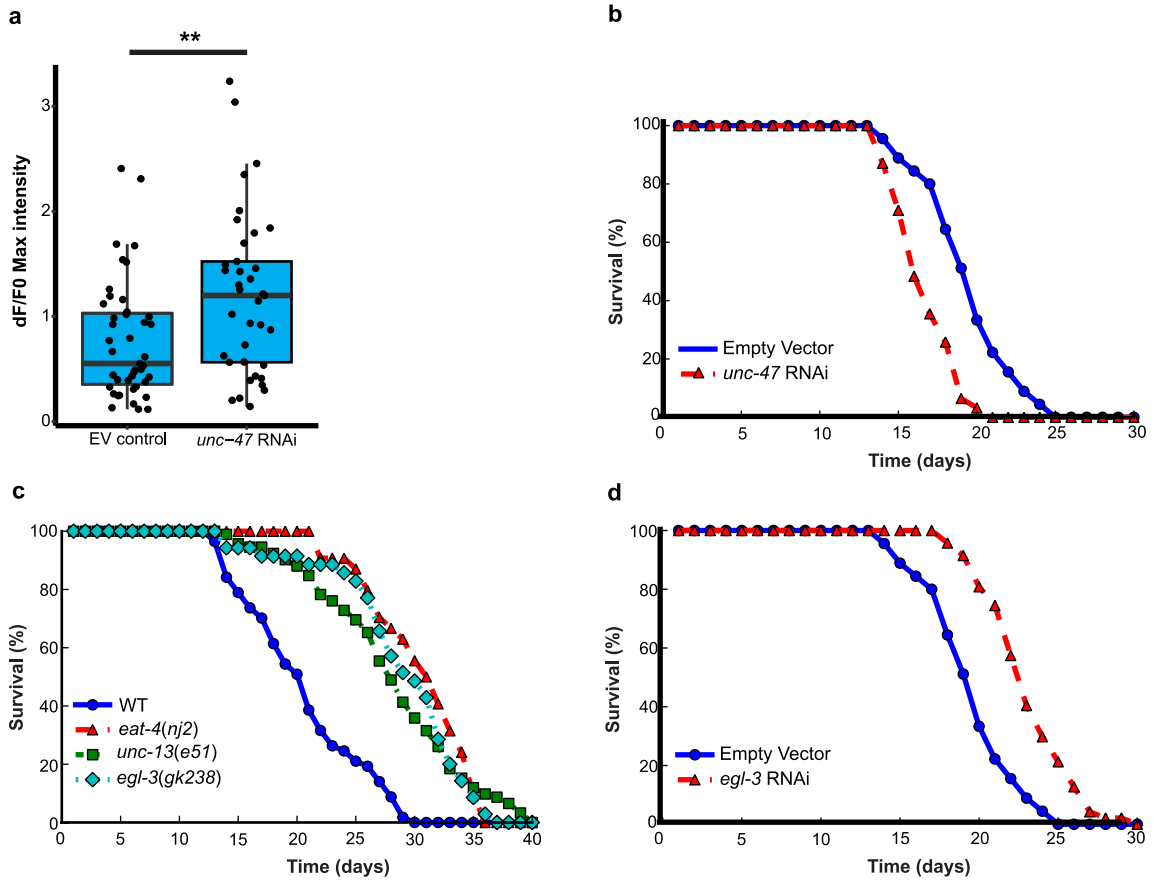

Extended Data Fig. 4 | Neural excitation, neuropeptide signalling and lifespan in *C. elegans*. **a**, Increased excitation of ASH neurons following RNAi against the GABA vesicular transporter *unc-47*. GCaMP imaging was performed on worms with enhanced neuronal RNAi (see Fig. 3 legend and Methods) for *unc-47* ($n = 37$) or controls ($n = 43$) at day 2. $^{**}P = 6.8 \times 10^{-3}$ by Mann–Whitney *U*-test. **b**, RNAi of *unc-47* reduces lifespan. Worms with enhanced neuronal RNAi were treated with *unc-47* ($n = 31$) or control RNAi ($n = 84$). Shown is a representative lifespan analysis replicated three times. $P = 1.3 \times 10^{-6}$ by log-rank test. **c**, Reduction in synaptic neurotransmission or neuropeptide signalling extends lifespan in *C. elegans*. Mutations in genes affecting glutamatergic neurotransmission (*eat-4*), presynaptic function (*unc-13*) and neuropeptide signalling (*egl-3)* produce comparable lifespan extensions. WT, $n = 57$; *eat-4(nj2)*, $n = 54$, $P \leq 2.2 \times 10^{-16}$; *unc-13(e51)*, $n = 92$, $P = 3.6 \times 10^{-14}$; *egl-3(gk238)*, $n = 35$, $P = 8.3 \times 10^{-11}$ by log-rank test. Curves are representative of two independent replicates. **d**, Extension of lifespan by *egl-3* RNAi in worms with enhanced neuronal RNAi. Shown are lifespan curves representative of two independent replicates. *egl-3* RNAi ($n = 47$ worms); empty vector ($n = 84$ worms). $P = 3.5 \times 10^{-11}$ by log-rank test.

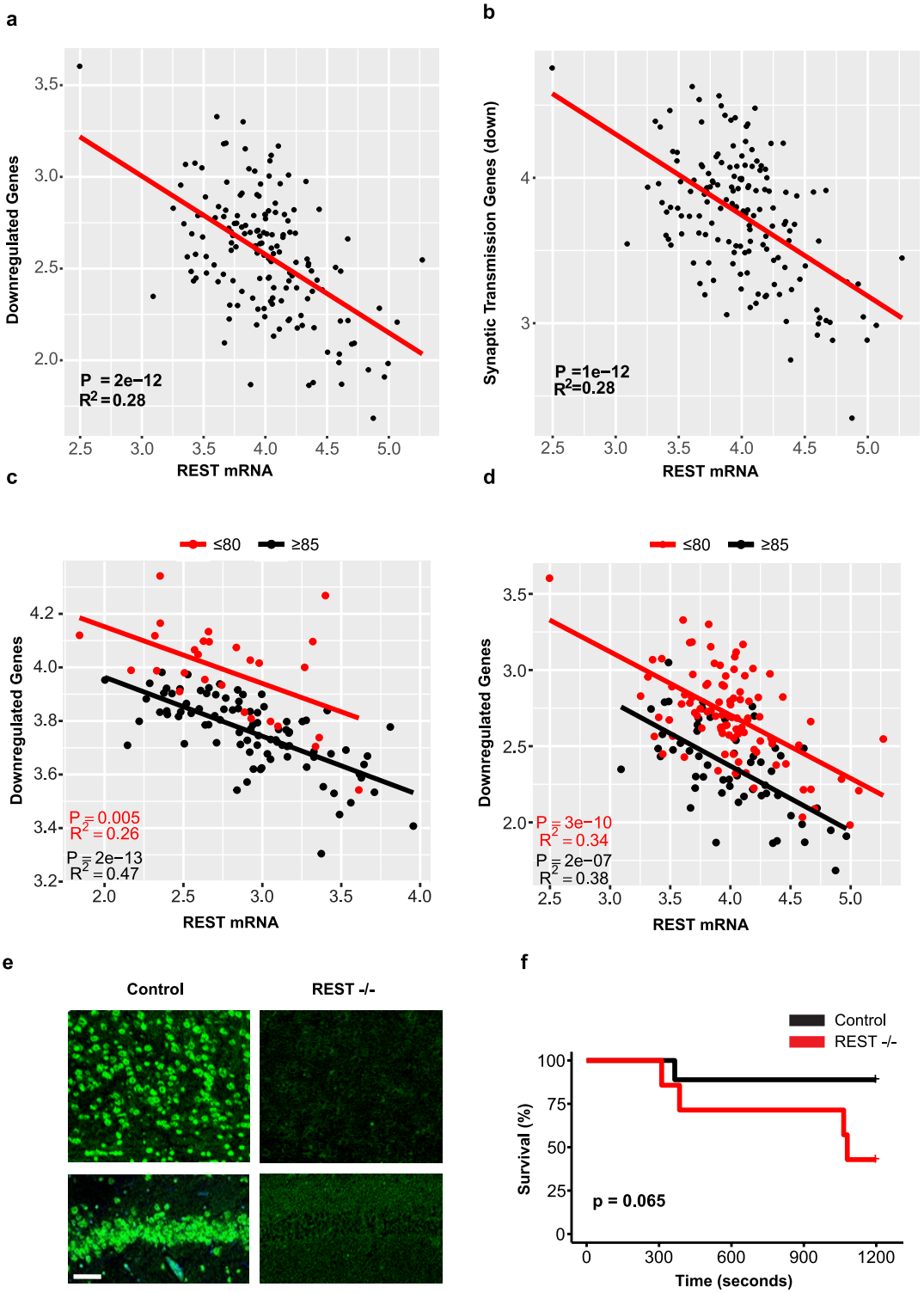

Extended Data Fig. 5 | Gene regulation and neural activity associated with REST and extended longevity. a, **b**, Expression of genes that are downregulated in individuals ≥85 years old versus ≤80 years old is inversely related to *REST* mRNA levels. Shown is linear regression analysis of normalized and adjusted *REST* mRNA levels and mean expression of all downregulated genes (**a**) and downregulated genes associated with the synaptic transmission GO term (**b**). Data are from the CMC cohort. Each point represents an individual case, $n = 155$ individuals. *P* values derived by a *t*-test for the slope of the regression line. Note similarity to the data for the ROSMAP cohort in Fig. 2a, b. **c**, **d**, Stratification by age group. Analysis of the ROSMAP cohort (**c**, $n = 117$ individuals) and the CMC cohort (**d**, $n = 155$ individuals) as in Fig. 2a, but stratified by age group. *P* values derived by *t*-test for the slope of the regression line. **e**, Loss of REST expression in conditional *Rest* knockout mice. Representative images of the cortex (top) and hippocampus (bottom) from $Rest^{lx/lx}$ (control) and *Nestin-Cre*;$Rest^{lx/lx}$ ($Rest^{-/-}$) mice. Immunolabelling was performed with the anti-mouse REST-14 antibody directed against the REST C-terminal domain (Supplementary Table 20). Scale bar, 40 μm. Image is representative of an experiment replicated four times. **f**, Survival of $Rest^{-/-}$ and control mice following administration of the seizure-inducing agent PTZ (40 mg kg^{-1x}r $Rest^{-/-}$ versus control by log-rank test. Control, $n = 9$; $Rest^{-/-}$, $n = 7$.

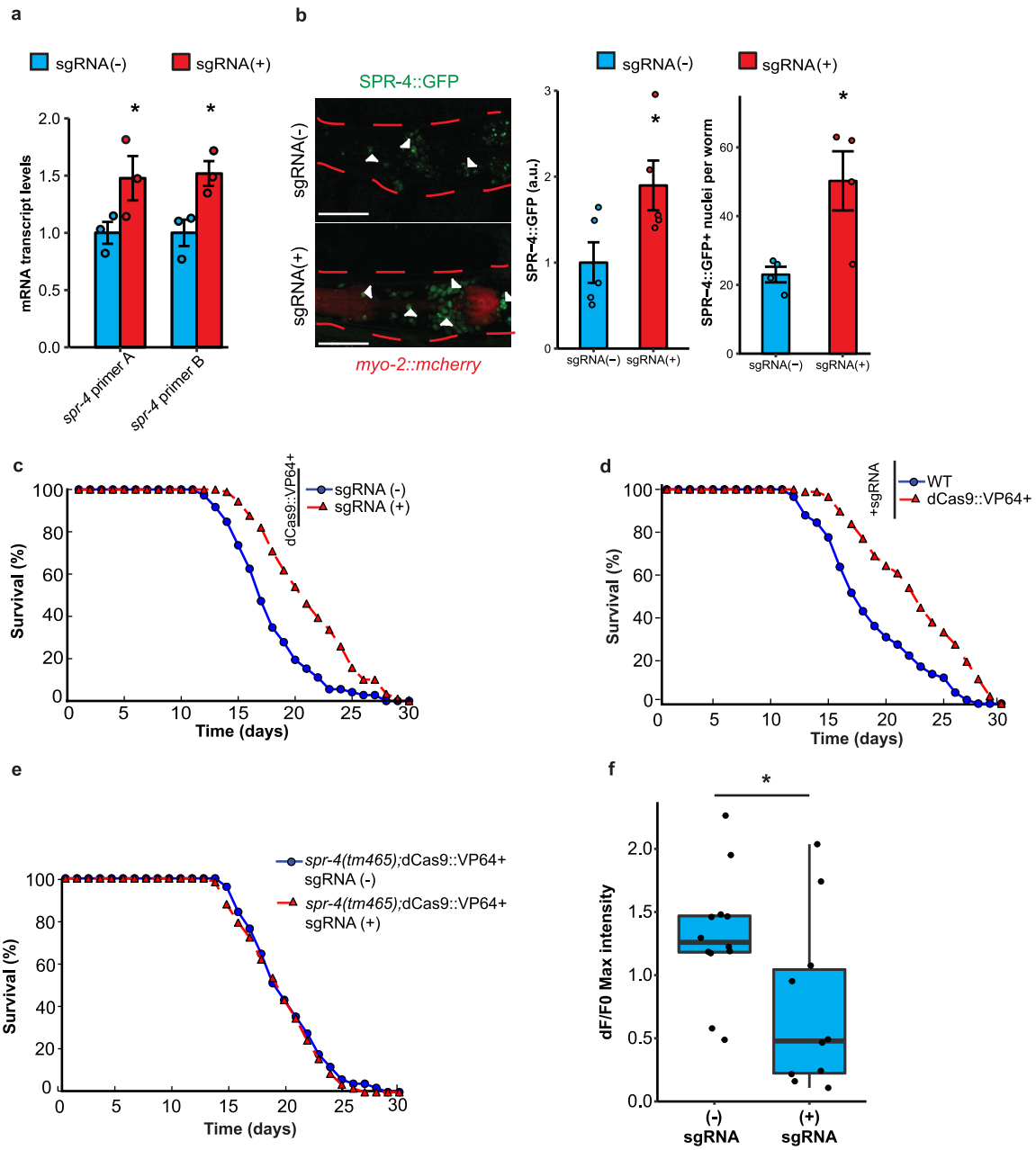

Extended Data Fig. 6 | Induction of *spr-4* extends lifespan and suppresses neural excitation in *C. elegans*. **a**, *spr-4* mRNA levels in worms expressing a stably integrated dCas9::VP64 transgene in the presence (sgRNA(+)) or absence (sgRNA(−)) of four different sgRNAs targeting the *spr-4* promoter. Transcript levels were determined by qRT–PCR and normalized to sgRNA(−) controls. Mean ± s.e.m., $n = 3$. Primer A, $^*P = 0.041$; primer B, $^*P = 0.020$ by one-sided Student's *t*-test. **b**, dCas9::VP64-mediated elevation of SPR-4 protein levels. Left, representative images of the head region of heterozygous F_1 progeny of the strains bearing a *pspr-4::spr-4::gfp::spr-4utr* transgene. Arrowheads indicate SPR-4::GFP-positive nuclei. Dashed red lines indicate the outline of the worm body. Scale bar, 40 μm. Middle, SPR-4::GFP protein levels are increased by dCAS9::VP64 mediated activation. Values represent mean ± s.e.m. sgRNA(−), $n = 5$ worms; sgRNA(+), $n = 5$ worms with 7–38 measurements per worm; $^*P = 0.022$, one-sided Student's *t*-test. Right, SPR-4::GFP expression appears in more cells following dCAS9::VP64-mediated activation. Values represent mean ± s.e.m. sgRNA(−), $n = 4$ worms; sgRNA(+), $n = 4$ worms. $^*P = 0.011$, one-sided Student's *t*-test. Shown is a representative experiment replicated three times. **c**, Extended lifespan in worms expressing an integrated *dCas9::VP64* transgene and sgRNAs targeting the *spr-4* promoter (sgRNA(+)) ($n = 79$ worms) relative to dCas9::VP64-expressing worms in the absence of sgRNAs (sgRNA(−)) ($n = 57$ worms). $P = 5.5 \times 10^{-9}$, log-rank test. Representative of an experiment replicated six times. **d**, Lifespans of worms expressing sgRNA targeting the *spr-4* promoter in the presence ($n = 87$ worms) or absence ($n = 58$ worms) of dCas9::VP64. $P = 3.7 \times 10^{-7}$, log-rank test. Representative of an experiment replicated twice. **e**, Lifespans of dCas9::VP64-expressing worms in the presence ($n = 51$ worms) or absence ($n = 58$ worms) of sgRNAs on the *spr-4(tm465)* loss-of-function mutant background. $P = 0.49$, log-rank test. Representative of three independent replicates. **f**, Overexpression of *spr-4* reduces neural excitation. GCaMP imaging was performed in ASH neurons in SPR-4-overexpressing (sgRNA(+)) and control (sgRNA(−)) worms in the lines described in **c**. Shown are maximum GCaMP fluorescence changes. sgRNA(−), $n = 12$ worms; sgRNA(+), $n = 10$ worms. $^*P = 0.025$, Mann–Whitney *U*-test.

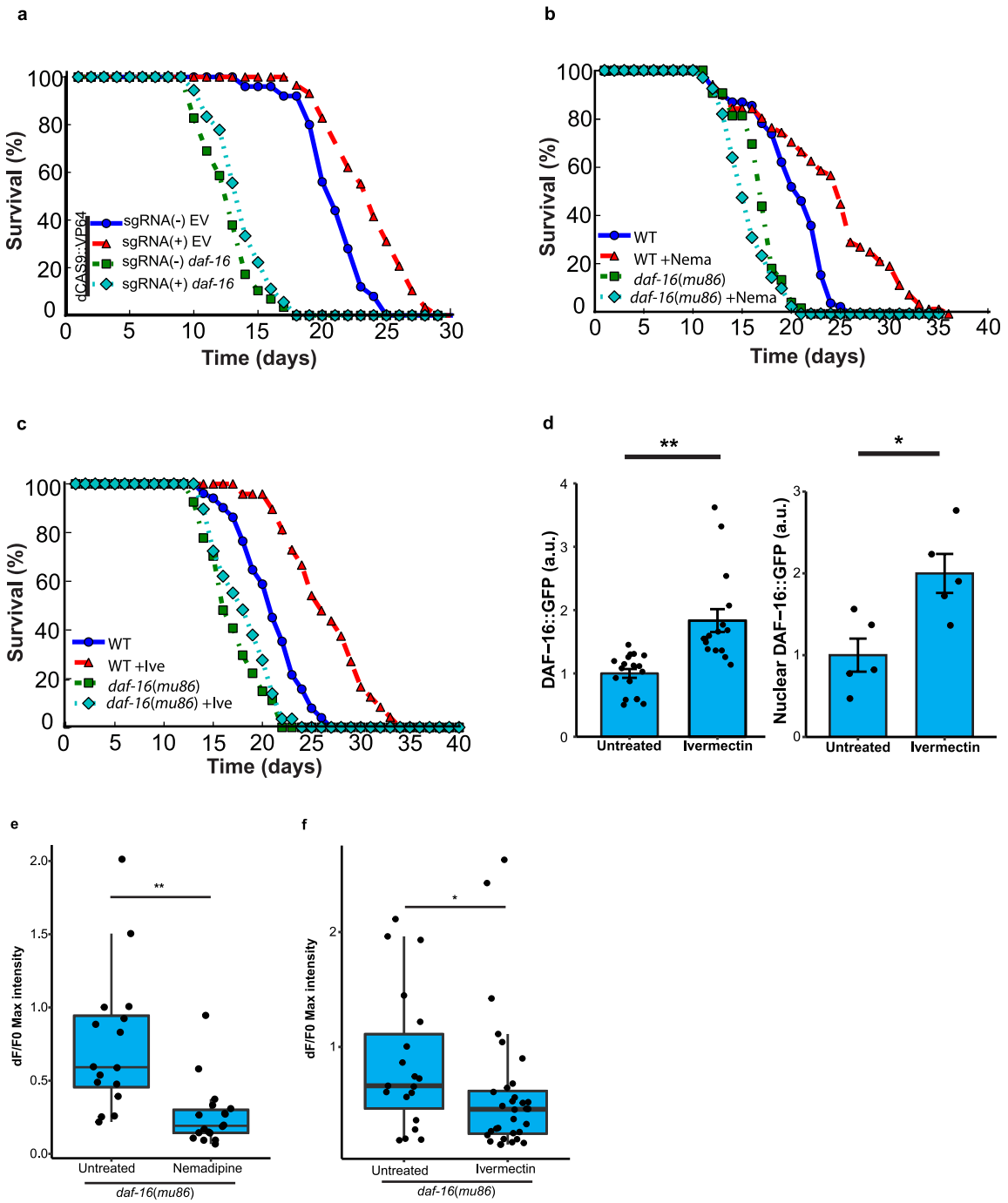

Extended Data Fig. 7 | Lifespan extension by overexpression of *spr-4* and inhibition of neural excitation depends on DAF-16. a, Extension of lifespan by overexpression of *spr-4* is dependent on DAF-16. Lifespans of worms overexpressing *spr-4* (sgRNA(+); dCAS9::VP64) or not overexpressing *spr*-4 (sgRNA(−); dCAS9::VP64) following treatment with *daf-16* RNAi or an empty vector control. sgRNA(+) EV ($n = 29$ worms) versus sgRNA(−) EV ($n = 25$ worms): $P = 2.7 \times 10^{-4}$; sgRNA(+) *daf-16* ($n = 18$ worms) versus sgRNA(−) *daf-16* ($n = 29$ worms): $P = 0.20$ by log-rank test. Representative of four independent replicates. **b**, **c**, Extension of lifespan by the inhibitors of neural excitation ivermectin and nemadipine is DAF-16-dependent. Shown are lifespan determinations for wild-type control and *daf-16*(*mu86*) mutant worms in the presence or absence of nemadipine (2 μM; **b**) or ivermectin (1 pg ml^{-1}; **c**). **b**, WT, $n = 69$ worms; WT + Nema, $n = 51$; *daf-16*, $n = 43$; *daf-16* + Nema, $n = 67$. WT + Nema versus WT, $P = 9.9 \times 10^{-8}$; *daf-16* + Nema versus *daf-16*, $P = 0.014$; log-rank test. **c**, WT, $n = 78$ worms; WT + Ive, $n = 77$; *daf-16*, $n = 27$; *daf-16* + Ive, $n = 29$. WT + Ive versus WT, $P = 7.3 \times 10^{-8}$; *daf-16* + Ive versus *daf-16*, $P = 0.22$; log-rank test. Curves are representative of an experiment replicated two (nemadipine) or three (ivermectin) times. **d**, Inhibition of neural excitation with ivermectin elevates DAF-16 levels. Worms expressing a *Daf-16::GFP* transgene were treated for 10 days with 1 pg ml^{-1} ivermectin and assessed by confocal microscopy. Left, total DAF-16::GFP (mean ± s.e.m.). Untreated, $n = 19$ worms; ivermectin, $n = 16$ worms. $^{**}P = 2.5 \times 10^{-7}$, Mann–Whitney *U*-test. Right, nuclear DAF-16::GFP. $n = 5$ worms per group, 50–61 nuclei per worm. $^{*}P = 0.013$ by Student's *t*-test. Results are representative of an experiment replicated twice. **e**, DAF-16 is not required for inhibition of neural excitation by nemadipine. Shown are maximum ASH GCaMP intensity changes for day 2 *daf-16*(*mu86*) mutant worms treated for 24 h with 2 μM nemadipine (untreated, $n = 16$ worms; nemadipine, $n = 18$ worms). $P = 9.4 \times 10^{-5}$, Mann–Whitney *U*-test. **f**, DAF-16 is not required for inhibition of neural excitation by ivermectin. Shown are data from day 2 worms treated for 24 h with 1 pg ml^{-1} ivermectin (control, $n = 19$ worms; ivermectin, $n = 32$ worms). $P = 0.030$, Mann–Whitney *U*-test.

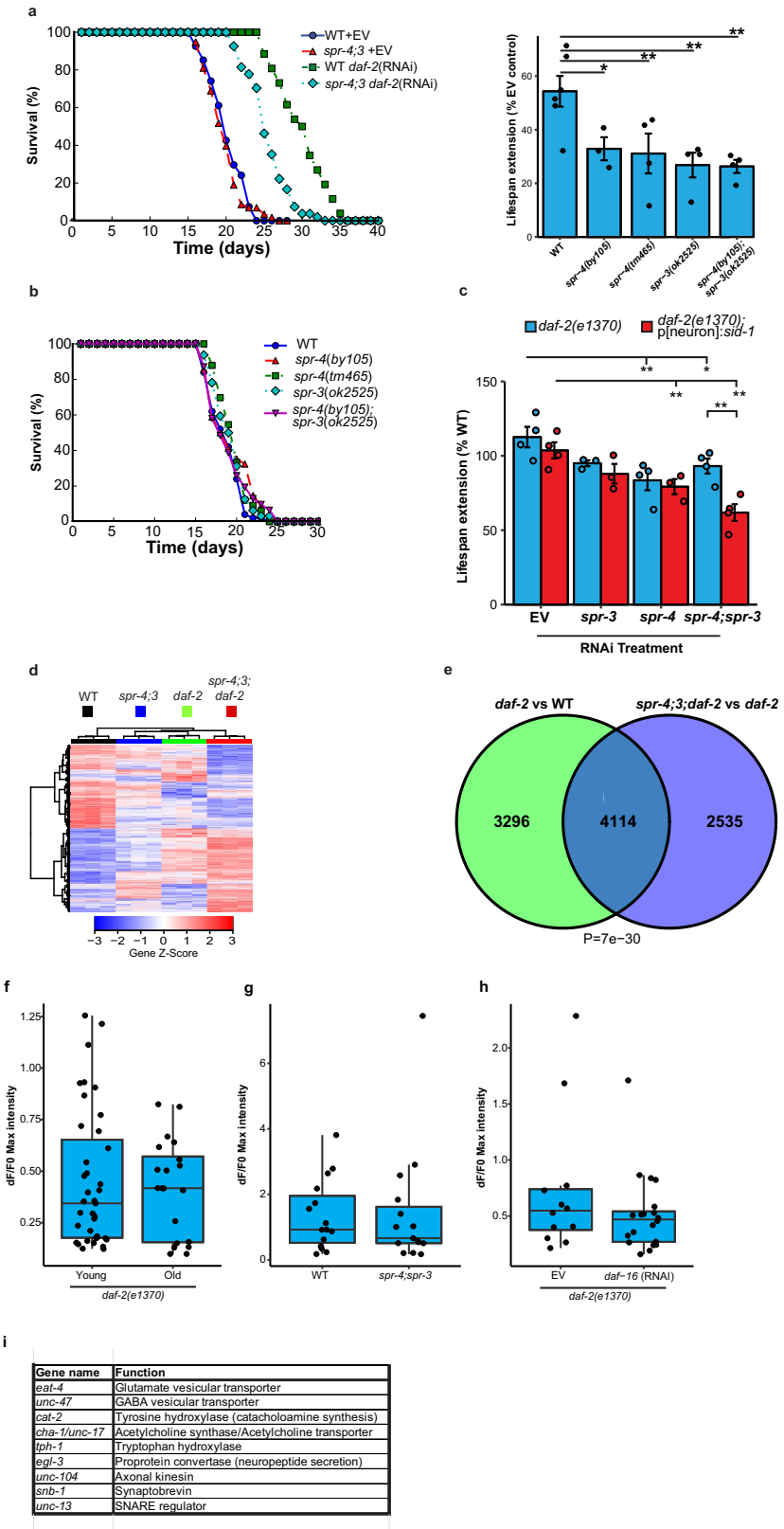

i

Gene name	Function
eat-4	Glutamate vesicular transporter
unc-47	GABA vesicular transporter
cat-2	Tyrosine hydroxylase (catacholoamine synthesis)
cha-1/unc-17	Acetylcholine synthase/Acetylcholine transporter
tph-1	Tryptophan hydroxylase
egl-3	Proprotein convertase (neuropeptide secretion)
unc-104	Axonal kinesin
snb-1	Synaptobrevin
unc-13	SNARE regulator

Extended Data Fig. 8 | See next page for caption.

Extended Data Fig. 8 | SPR-3 and SPR-4 contribute to lifespan extension and gene regulation associated with reduced DAF-2 and insulin–IGF-like signalling. a, Loss of function of SPR-3 and SPR-4 reduces the lifespan extension induced by *daf-2* RNAi. Left, representative lifespan analysis of *spr-4(by105);spr-3(ok2525)* double mutant and wild-type worms following *daf-2* or empty vector control RNAi. WT + EV, $n = 54$ worms; *spr-4;3* + EV, $n = 58$ worms; WT + *daf-2*, $n = 26$ worms; *spr-4;3* + *daf-2*, $n = 54$ worms. Right, values represent mean ± s.e.m. per cent lifespan extension (*daf-2* RNAi versus EV control) in the indicated genotypes. WT, $n = 6$ independent experiments; *spr-4*(*by105*), $n = 3$, $^{*}P = 0.017$ versus WT; *spr-4*(*tm465*), $n = 4$, $^{**}P = 0.0062$ versus WT; *spr-3*(*ok2525*), $n = 4$, $^{**}P = 0.0018$ versus WT; *spr-4*(*by105*);*spr-3*(*ok2525*), $n = 4$, $^{**}P = 0.0016$ versus WT; Students *t*-test. See Supplementary Table 22 for individual lifespan data and statistics. **b**, Lifespan is unaffected by *spr-4* and *spr-3* mutations in a wild-type background. WT, $n = 50$ worms; *spr-3*(*ok2525*), $n = 31$; *spr-4*(*by105*);*spr-3*(*ok2525*), $n = 32$; *spr-4*(*by105*), $n = 34$; *spr-4*(*tm465*), $n = 33$.There were no reproducibly significant changes by the log-rank test in 3–6 independent experiments per genotype (see Supplementary Table 22). **c**, Quantification of lifespan extension in *daf-2* mutant worms shown in Fig. 3b attributable to neuronal expression of *spr-3* and *spr*-4. RNAi was targeted to neurons by neuronal expression of a *sid-1* transgene in otherwise *sid-1*-null *daf-2(1370)* mutants (*daf-2*;p[neuron]:*sid-1*), and compared with untargeted RNAi in *sid-1* wild-type *daf-2(1370)* mutants (*daf-2*). Values represent mean ± s.e.m. lifespan extension relative to the control *sid-1*(*pk3321*);p[neuron]:*sid-1* worms treated with empty vector ($n = 3$ independent experiments). Significant lifespan effects were not observed for RNAi in the absence of the *daf-2* mutation. $^{*}P < 0.05$; $^{**}P < 0.01$ by Student's *t*-test. **d**, Gene expression determined by RNA-seq in day 2 adult worms. Differentially expressed genes (rows) and the indicated worm genotypes (columns) were clustered, and gene expression, transformed to a *z*-score per gene, is represented in a heat map. $n = 3$ independent replicates per genotype. **e**, Venn diagram illustrating the overlap in differentially expressed genes in *daf-2* single mutant versus WT and *spr-4;spr-3;daf-2* triple mutant versus *daf-2* single mutant worms. $P = 7 \times 10^{-30}$, Fisher's exact test with a one-sided alternative hypothesis. **f**, Long-lived *daf-2* mutants do not show an age-related increase in neural excitation. Shown are maximum ASH GCaMP intensity changes in day 1–2 ($n = 39$) and day 14–16 ($n = 20$) *daf-2(e1370)* mutant worms. Note the absence of the age-related increase in excitation observed in wild-type ageing worms (Fig. 1e). $P = 0.93$, Mann–Whitney *U*-test. **g**, The *spr-4;spr-3* double mutation in a wild-type background does not significantly affect neural excitation in ASH neurons. WT, $n = 15$ worms; *spr-4;spr-3*, $n = 15$ worms. $P = 0.62$, Mann–Whitney *U*-test. **h**, DAF-16 does not mediate suppression of neural excitation in the *daf-2* mutant. RNAi against *daf-16* was performed in *daf-2(e1370)* mutant worms on a *sid-1*(*pk3321*);p[neuron]:*sid-1* background to augment RNAi in neurons (*daf-16* RNAi, $n = 20$ worms, EV control, $n = 12$ worms). $P = 0.33$, Mann–Whitney *U*-test. **i**, Descriptions of the genes targeted by RNAi in Fig. 4d.

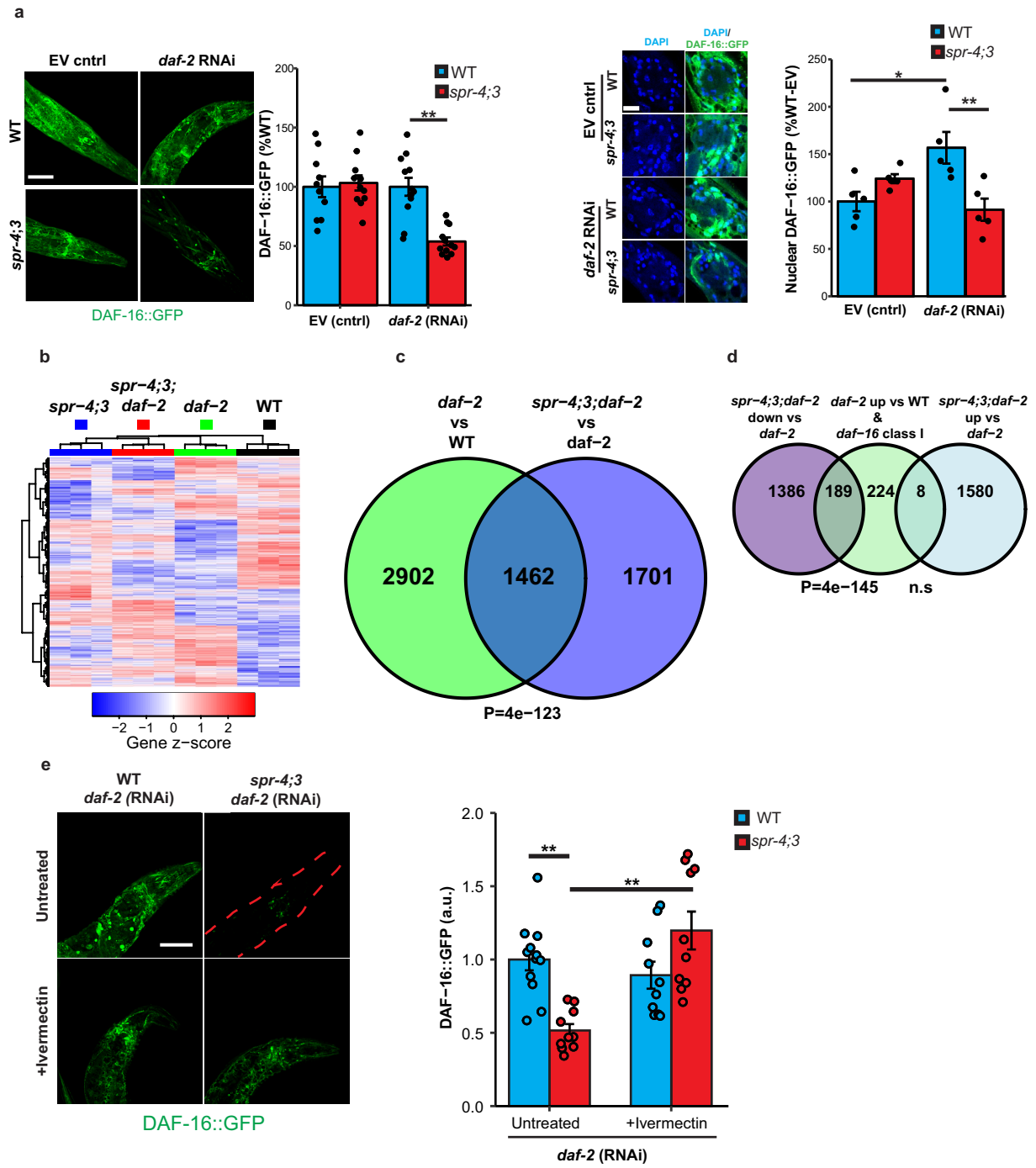

Extended Data Fig. 9 | See next page for caption.

Extended Data Fig. 9 | Regulation of DAF-16 by SPR-3 and SPR-4. **a**, Reduced DAF-16 activation in *spr-4;spr-3* mutants following *daf-2* RNAi. Left confocal image, day 10 worms of the indicated genotypes expressing an integrated *Daf-16::GFP* transgene and treated with *daf-2* RNAi or empty vector control since day 1 of adulthood. Images are maximum intensity *z*-projections. Scale bar, 40 μm. Left bar graph, mean ± s.e.m. GFP intensity in the peri-pharyngeal regions of *spr-4;spr-3* double mutants relative to wild-type controls for a representative experiment replicated four times (see Methods for details of analysis). $n = 8$–12 worms per replicate. $^{**}P = 5.2 \times 10^{-5}$, Welch's *t*-test. Right confocal image, higher-magnification views of DAF-16::GFP and DAPI-labelled nuclei. Images are magnified confocal *z*-planes. Scale bar, 10 μm. Right bar graph, mean ± s.e.m. nuclear GFP intensity relative to the WT-EV control, $n = 5$ worms per genotype and 51–89 nuclei per worm. $^{*}P = 0.016$, $^{**}P = 5.5 \times 10^{-3}$ by ANOVA with post hoc Tukey test. Values and images are representative of an experiment replicated three times. **b**, Gene expression determined by RNA-seq in adult day 10 worms. Differentially expressed genes (rows) and replicates of the indicated worm genotypes (columns) were clustered, and gene expression, transformed into a *z*-score per gene, is represented in a heat map. $n = 3$ independent replicates per genotype. **c**, Venn diagram illustrating the overlap of differentially expressed genes in day 10 *daf-2* versus wild-type and *spr-4;spr-3;daf-2* versus *daf-2* worms. $P = 4 \times 10^{-123}$, Fisher's exact test with a one-sided alternative hypothesis. **d**, Overlap of class I *daf-16* target genes (see Methods) with genes downregulated in day 10 *spr-4;spr-3;daf-2* triple mutants relative to *daf-2* single mutants. *P* values calculated using a hypergeometric distribution (see Methods). n.s., $P = 0.99$. **e**, Ivermectin increases DAF-16::GFP levels in *spr-4;spr-3* worms following *daf-2* RNAi. Left, confocal imaging of GFP fluorescence in ivermectin-treated (10 pg ml^{-1}) and untreated worms. The red dashed lines indicate the worm body. Right, quantification of DAF-16::GFP (mean GFP intensity ± s.e.m., WT/Untreated, $n = 12$; WT/Ivermectin, $n = 10$; *spr-4;spr-3*/Untreated, $n = 10$; *spr-4;spr-3*/Ivermectin, $n = 10$. $^{**}P = 4.6 \times 10^{-4}$ (*spr-4;spr-3* versus WT/untreated), $P = 2.6 \times 10^{-4}$ (*spr-4;spr-3*/Ivermectin versus *spr-4;spr-3*/untreated) by Mann–Whitney *U*-test with multiple testing correction by Holm's method. Shown is a representative experiment replicated three times.

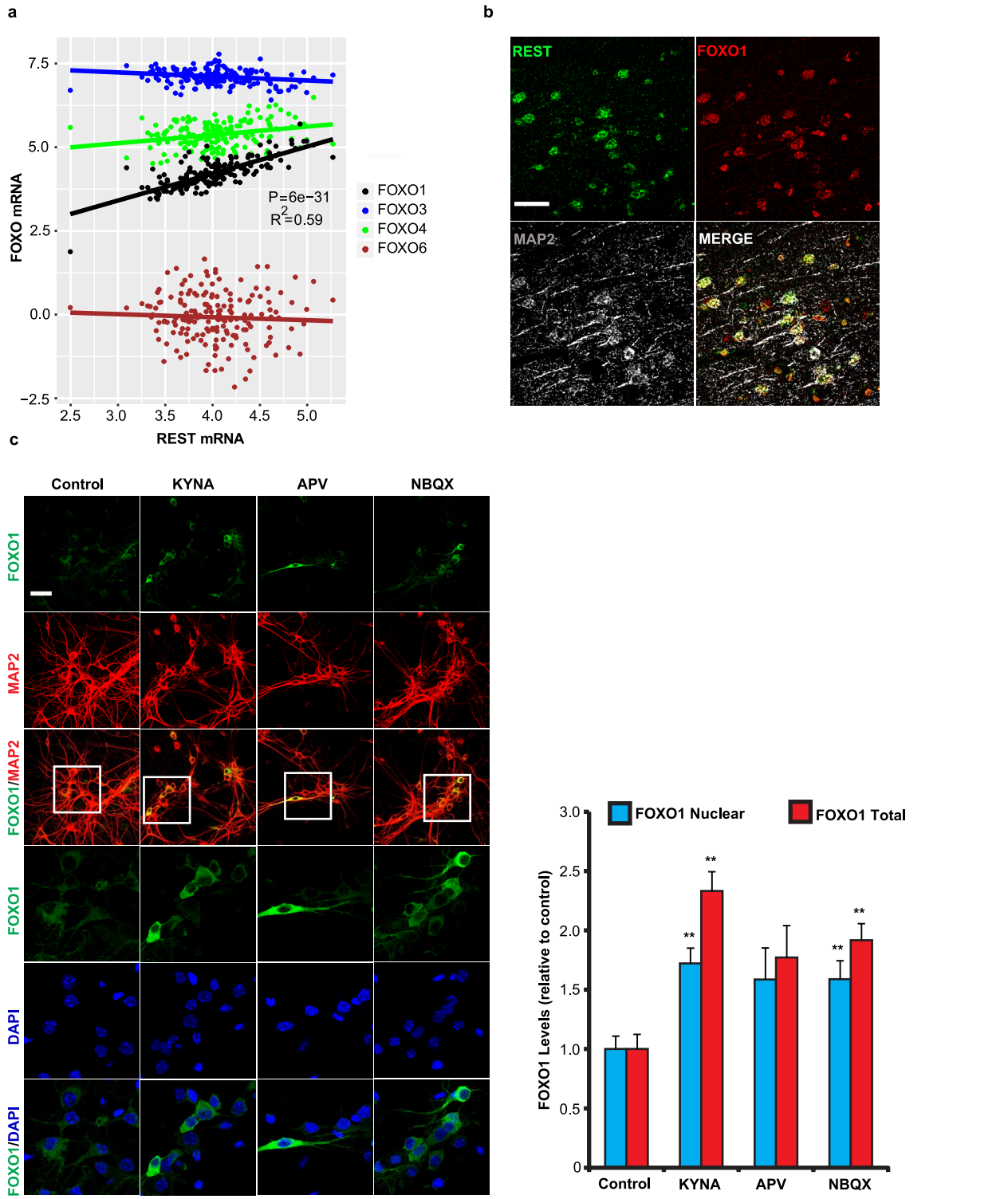

Extended Data Fig. 10 | Coregulation of FOXO1 and REST in the ageing brain and modulation by glutamatergic signalling. a, Linear regression analysis of *REST* and *FOXO* mRNA levels in the prefrontal cortex of 174 cognitively intact individuals (age ≥60 years) from the CMC cohort determined by RNA-seq. *P* values derived from a *t*-test for the slope of the regression line and Bonferroni-corrected across all expressed genes. **b**, Colocalization of REST and FOXO1 in neurons of the aged human prefrontal cortex. Confocal immunofluorescence microscopy was performed in human prefrontal cortex using antibodies against REST (green, rabbit polyclonal; Bethyl), FOXO1 (red, goat polyclonal; LS-Bio) and the neuronal marker MAP2 (grey, chicken polyclonal; Abcam). Scale bar, 40 μm. The image shown is representative of immunofluorescence labelling performed in 30 individuals. See Supplementary Table 20 for additional information on antibodies. **c**, Inhibition of glutamatergic signalling in mouse cortical neuronal cultures elevates FOXO1 levels. Left, primary mouse cortical neuronal cultures treated with kynurenic acid (KYNA, 5 μM), AP5 (50 μM), NBQX (2 μM) or vehicle control were analysed by confocal immunofluorescence for FOXO1 or MAP2 and labelled with DAPI. Boxed areas are magnified in the lower three rows. Note that most FOXO1 in cultured neurons is cytoplasmic, but a detectable nuclear component overlaps with DAPI. Scale bar, 40 μm. Right, quantification (mean ± s.e.m.) of total and nuclear FOXO1 levels in MAP2-positive neurons. Control, $n = 200$; KYNA, $n = 326$; AP5, $n = 148$; NBQX, $n = 197$. FOXO1 total/KYNA, $^{**}P = 2.1 \times 10^{-8}$; FOXO1 nuclear/KYNA, $^{**}P = 1.1 \times 10^{-4}$; FOXO1 total/NBQX, $^{**}P = 8.8 \times 10^{-13}$; FOXO1 nuclear/NBQX, $^{**}P = 5.2 \times 10^{-6}$; Mann–Whitney *U*-test with multiple testing correction by Holm's method. Shown is a representative experiment replicated three times.